

Exciton-dominated Dielectric Function of Atomically Thin MoS₂ Films

Yiling Yu², Yifei Yu¹, Yongqing Cai³, Wei Li⁴, Alper Gurarslan^{1,5}, Hartwin Peelaers⁶
David E. Aspnes², Chris G. Van de Walle⁶, Nhan V. Nguyen⁴, Yong-Wei Zhang³, Linyou Cao^{1,2*}

¹Department of Materials Science and Engineering, North Carolina State University, Raleigh, NC 27695, USA;

²Department of Physics, North Carolina State University, Raleigh NC 27695, USA; ³Institute of High Performance Computing, A*STAR, Singapore 138632; ⁴Semiconductor and Dimensional Metrology Division, National Institute of Standards and Technology, Gaithersburg, Maryland 20899, USA; ⁵Department of Fiber and Polymer Science, North Carolina State University, Raleigh, NC 27695, USA; ⁶Materials Department, University of California, Santa Barbara, CA 93106, USA

Abstract

We systematically measure the dielectric function of atomically thin MoS₂ films with different layer numbers and demonstrate that excitonic effects play a dominant role in the dielectric function when the films are less than 5-7 layers thick. The dielectric function shows an anomalous dependence on the layer number. It decreases with the layer number increasing when the films are less than 5-7 layers thick but turns to increase with the layer number for thicker films. We show that this is because the excitonic effect is very strong in the thin MoS₂ films and its contribution to the dielectric function may dominate over the contribution of the band structure. We also extract the value of layer-dependent exciton binding energy and Bohr radius in the films by fitting the experimental results with an intuitive model. The dominance of excitonic effects is in stark contrast with what reported at conventional materials whose dielectric functions are usually dictated by band structures. The knowledge of the dielectric function may enable capabilities to engineer the light-matter interactions of atomically thin MoS₂ films for the development of novel photonic devices, such as metamaterials, waveguides, light absorbers, and light emitters.

* To whom correspondence should be addressed.

Email: lcao2@ncsu.edu

Two-dimensional (2D) transition metal dichalcogenide (TMDC) materials have been known exhibiting strong exciton binding energy that may be one order of magnitude larger than conventional

semiconductor materials¹⁻⁶. However, how the extraordinarily strong exciton binding energy could affect the light-matter interactions such as dielectric functions of the materials has remained unexplored. The lack of knowledge about the dielectric function has significantly limited the application of 2D TMDC materials in many exciting photonic fields such as metamaterials⁷, which relies on the sophisticated manipulation of effective dielectric functions to enable novel optical functionalities. In this work we have measured the dielectric function of atomically thin MoS₂ films and discovered that it is dominated by the effect of the tightly bound excitons, as evidenced by an anomalous dependence of the dielectric function on the layer number. The dielectric function decreases with the layer number increasing when the MoS₂ films are less than 5 layers thick, but turn to increase with the layer number for thicker. We also quantitatively evaluate the exciton binding energy and Bohr radius of the thin films by fitting the experimental results with an intuitive model. The observed dominance of excitonic effects in the dielectric function is in stark contrast with what expected at conventional materials, whose dielectric functions are usually dictated by band structures^{8,9}. Our success in this discovery is built upon a unique self-limiting chemical vapor deposition (CVD) process that we have recently developed¹⁰. The self-limiting CVD process can be used to grow centimeter-scale, uniform, and high quality atomically thin MoS₂ films with controlled layer numbers and remarkable uniformity (Fig. S1-S5). This allows us to examine the dielectric function of MoS₂ films as a function of well-defined layer numbers. Our work is different from earlier research for the dielectric function of MoS₂ films^{11, 12}, whose results are likely inaccurate due to the lack of satisfactory uniformity or precise control of the layer number.

We measured the dielectric function ($\epsilon_1 + i\epsilon_2$) of as-grown MoS₂ films on sapphire substrates using spectroscopic ellipsometry¹³. Fig. 1a-b shows the real ϵ_1 and imaginary ϵ_2 parts of the dielectric function in the visible range that are derived from experimental measurements (see Fig. S7-S8 for the fit between experimental and simulated results). Owing to the extreme geometrical anisotropy of the film,

what we obtained is actually the in-plane component of the dielectric tensor because the out-of-plane dielectric function may only contribute trivially to the optical response due to the difficulty in exciting the vertical dipole of the atomically thin film¹³. As further evidence for the measured in-plane dielectric function, we performed the spectroscopic ellipsometry at different incident angles (40°-75°), and all of them ended up with giving very similar dielectric functions. The dielectric function of bulk MoS₂ is also measured and plotted in Fig. 1a-b as a reference, the result of which is consistent with what reported previously¹⁴. The three peaks in the spectral dielectric function can be assigned to *A*, *B*, and *C* from low to high energies, respectively¹⁵⁻¹⁸. The *A* and *B* peaks are related with the transition from the spin-orbit split valence bands to the lowest conduction band at the *K* and *K'* points, while the *C* peak is associated with the transition from the valence band to the conduction band at the part of the Brillouin zone between the *A* and Γ point^{16, 17}.

The measured dielectric function is not sensitive to the synthetic process or the substrate. The dielectric functions measured from the MoS₂ grown by using MoCl₅ and S as the precursors¹⁰ and by using MoO₃ and S as the precursors¹⁹ are essentially identical (Fig. S9a). We also find that the dielectric functions of the as-grown MoS₂ films on sapphire substrates and those transferred onto SiO₂/Si substrates are identical (Fig. S9b). Additionally, the dielectric function of the film is stable under ambient environment. We monitored the dielectric function of the as-grown MoS₂ films on sapphire substrates as a function of the time for the films to be exposed to ambient environment. We monitored the dielectric function of the films exposed to ambient environment for more than one week and found no change in the measured result (Fig. S10). The result we measured for the monolayer MoS₂ film is consistent with what previously measured using spectroscopic ellipsometry²⁰ but is 10-15% less than the results derived from absorption spectra²¹. We do like to point out some difference in the spectroscopic ellipsometry used by us as well as Ref. 20 and the spectroscopic absorption technique used in Ref. 21.

Spectroscopic ellipsometry is the most established technique for the measurement of dielectric functions, in which two parameters are measured at each wavelength and the dielectric function can be uniquely determined in any spectrum range with the thickness information of the film independently determined by AFM. The dielectric function may be derived from spectroscopic reflection using the Kramer-Kronig relationship as well. But to precisely find out the dielectric function using the Kramer-Kronig relationship requires information of the absorption in the entire spectral range. In Ref. 21 the absorption of the monolayer in the range higher than 3 eV, whose value is not experimentally available, is assumed to be equal to that of the bulk counterpart. This assumption might overestimate the dielectric function to some degree. We believe this is likely the reason why our result is around 10-15% less than the result reported in Ref.21.

Significantly, the measured dielectric function shows an anomalous dependence on the layer number (Fig. 1a-b). It decreases with the layer number increasing when the film is less than 5-7 layers thick and then turns to increase with the layer for thicker films. We were very careful to ensure no artifact introduced in the measurement. More specifically, we performed extensive AFM for each of the films studied prior to the ellipsometry measurement and confirmed the atomic-scale smoothness (roughness usually < 0.5 nm except the 8L, 9L and 10L films, whose roughness is a little bit larger in the range of 0.7-0.9 nm, see Fig. S1-S5) and excellent uniformity of the film. Additionally, for the result of each layer number, we measured at least three different sets of samples and observed only minor variation (5%) in the resulting dielectric function. To further illustrate this anomalous layer-dependence, we extract the imaginary part of the dielectric functions at the *A*, *B*, and *C* peaks from Fig. 1b and plot it as a function of the layer number (Fig.1c). The result clearly shows a decrease and then an increase in the dielectric function with the layer number continuously increasing from one. The layer dependence is similar for all the *A*, *B*, and *C* peaks (Fig. 1d). Given the similarity in the layer

dependence, we only focus on the *C* peak in the following discussion.

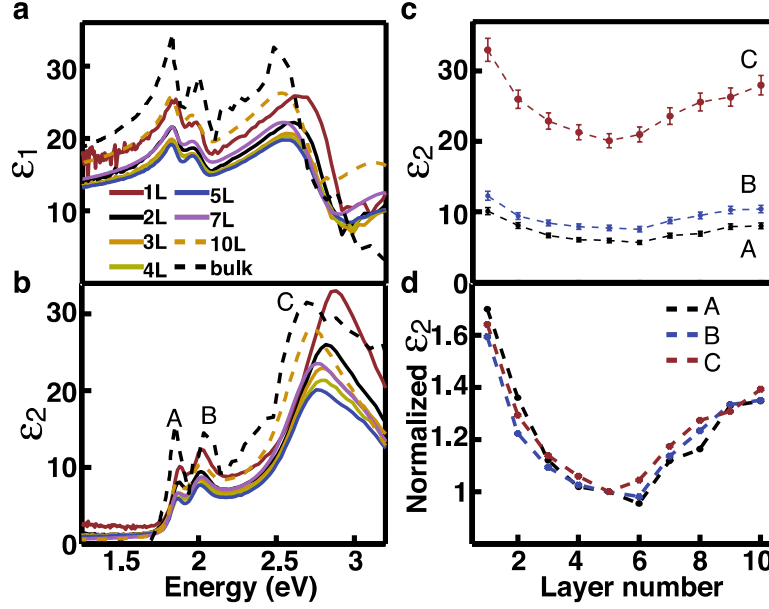


Figure 1. Anomalous layer-dependence of the dielectric function of 2D MoS₂. (a-b) Real and imaginary parts of the dielectric function of 2D MoS₂ vs. layer number. Also given is the dielectric function of bulk MoS₂. The three peaks can be assigned to *A*, *B*, and *C* excitons as labeled. Corresponding refractive indexes of the films are given in Figure S6 and Table S1 of the Supplementary Information. (c) The dependence of the imaginary part ϵ_2 of the dielectric function at the *A*, *B*, and *C* peaks on layer number. The error bar is 5% and estimated from the measurement results of multiple samples. (d) Normalized ϵ_2 at the *A*, *B*, and *C* peaks vs. layer number. The normalization is performed with respect to the corresponding value of each peak in the 5-layer MoS₂. Error bar is ignored for visual convenience.

To obtain physical insights into the observed layer dependence, we examine the dielectric function from the perspective of quantum mechanics. We only focus on the imaginary part ϵ_2 because the real part ϵ_1 can be deterministically correlated to ϵ_2 by the well-established Kramer-Kronig equation²². Fundamentally, ϵ_2 is related with interband transitions as^{8, 22, 23}

$$\epsilon_2(\omega) = \frac{4\pi^2 e^2}{m_0^2 \omega^2} J_{cv} |p_{cv}|^2 |U(0)|^2 \frac{\Gamma/2}{(E_{cv} - \hbar\omega)^2 + (\Gamma/2)^2} \quad (1)$$

where ω is the frequency, \hbar is the Planck's constant, e and m_0 are the charge and mass of free electrons, J_{cv} is the joint density of the initial (valence band) and final (conduction band) states involved in the transition. p_{cv} is an optical matrix element indicating the probability of the transition from the initial to final states. It consists of an integral over a unit cell that involves the momentum operator as well as the

unit cell wavefunctions in the conduction and valence bands. $|U(0)|^2$ represents the effect of excitons on the oscillator strength of the interband transition, where U is the relative motion wavefunction of the electrons and holes bound by Coulomb interactions and θ indicates the physical overlap of the electron and hole wavefunctions. E_{cv} is the optical energy gap between the conduction and valence bands involved and Γ is a damping constant determining the bandwidth of the interband transition.

For simplicity, we only focus on the dielectric function at the peak position (on-resonance) as shown in Fig. 1c-d, where $E_{cv} - \hbar\omega = 0$ and eq.(1) can be simplified as

$$\varepsilon_2(\omega) = \frac{4\pi^2 e^2}{m_0^2 \omega^2} J_{cv} |p_{cv}|^2 |U(0)|^2 \frac{2}{\Gamma} \quad (2)$$

Physically, Γ represents the width of the peak. From Fig. 1b the peak can be found phenomenally remaining to be similar in the films with different layer numbers. Therefore, it is reasonable to consider that Γ is independent of the layer number. The optical matrix element p_{cv} is also independent of the layer number because it is only related with unit cells and unit cell wavefunctions, both of which are not dependent on the layer number. The independence of p_{cv} on geometrical features has previously been demonstrated at quantum wells²⁴. Therefore, eq. (2) can be further simplified as

$$\varepsilon_2(\omega) = A_0 J_{cv} |U(0)|^2 \quad (3)$$

where A_0 includes all the terms independent of the layer number. Eq. (3) indicates that the layer dependence of the dielectric function may result from only two parameters: the joint density of states J_{cv} and the excitonic effect $|U(0)|^2$.

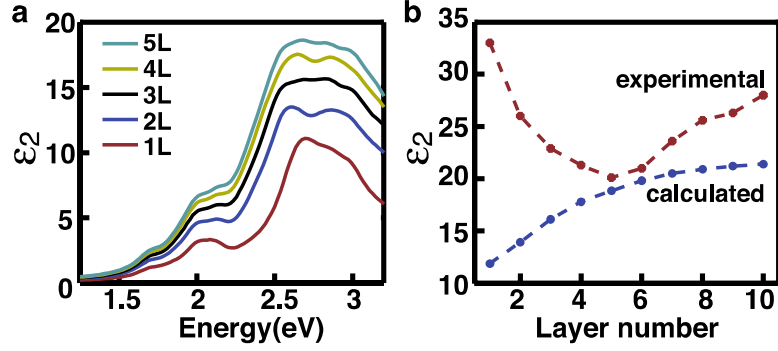


Figure 2. Comparison of the measured and calculated dielectric function of 2D MoS₂. (a) Calculated imaginary part ϵ_2 of the dielectric function of MoS₂ with different thickness. (b) Comparison of experimental and calculated results for ϵ_2 at the C peak as a function of the layer number. The error bar in the experimental result is ignored for visual convenience.

We can get more insight by further examining the specific layer dependence of the two parameters J_{cv} and $|U(0)|^2$. The joint density of states J_{cv} is determined by the band structure and expected to monotonically increase with the layer number. This is because the density of states in 2D materials is well known to be smaller than that in 3D materials^{8, 22} and the increase of the layer number in effect enables a continuous evolution from two dimensions (monolayers) to three dimensions (bulk). To quantitatively elucidate the layer dependence of J_{cv} , we calculate the ϵ_2 of MoS₂ films using density functional theory (DFT) techniques without considering excitonic effects¹⁸. The calculation result is given in Fig. 2a and essentially represents the density of states J_{cv} . It reproduces the major spectral features of the experimental results and indeed shows a monotonic increase with the layer number. For the convenience of comparison, we plot the calculated and measured dielectric functions at the C peak as a function of the layer number in Fig. 2b. The calculated results are understandably smaller than the experimental results due to the exclusion of excitonic effects. Of our interest is to compare the layer dependence in the calculated and experimental results. The similarity of the two results for the films > 5L suggests that the observed layer-dependent increase in the dielectric function in the relatively thicker

films may be correlated to the effect of the density of states J_{cv} . However, for the films less than 5 layers thick the calculated layer-dependence is opposite to the experimental observation (Fig.2b). This can be correlated to the other parameter not considered in the calculation, the excitonic effect $|U(0)|^2$. The excitonic effect is expected to be strong and to quickly decrease with the layer number due to the well known layer-dependent exponential decrease of exciton binding energy¹⁵.

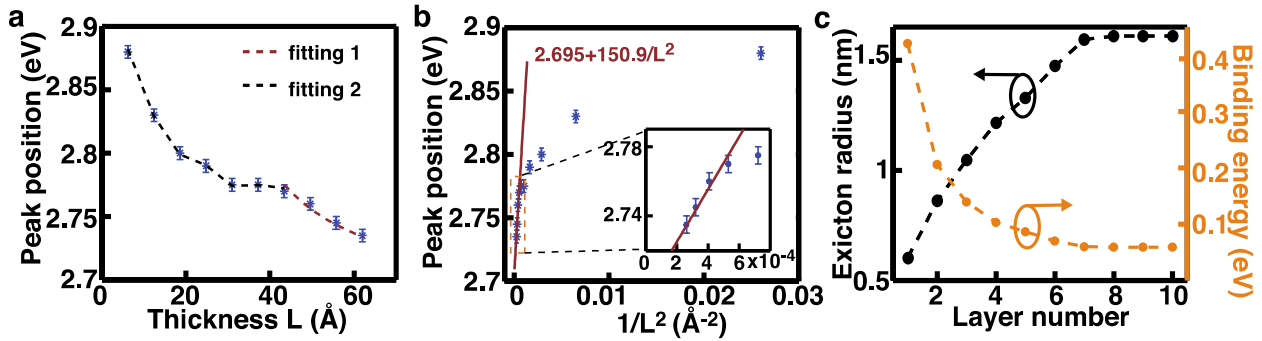


Figure 3. Strong, layer-dependent excitonic effects in atomically thin MoS₂ films. (a) The position of the *C* peak in MoS₂ films as a function of the thickness of the film L . The error bar ± 0.005 eV results from the possible errors in determining the peak position. The dashed lines are the fitting results using the model of infinite quantum wells (fitting 1) and the quantum well in fraction space (fitting 2) (b) The position of the *C* peak in MoS₂ films as a function of $1/L^2$, where L is the thickness of the film. The red line is the fitting results using the model of infinite quantum well with the fitting equation given as shown. The inset is a magnified version of the area indicated by the dashed yellow rectangle. (c) The dependence of the binding energy and exciton radius in MoS₂ films on the layer number.

The layer-dependent excitonic effect can be understood more quantitatively by examining the excitonic peak position with an intuitive model that involves quantum confinement and exciton binding energy. Of our interest is to quantitatively evaluate the layer dependence of the exciton binding energy from the observed evolution of the *C* exciton peak position with the layer number (Fig. 3a). The excitonic peak position (i.e. optical bandgap) is equal to the electronic bandgap minus the exciton binding energy, and its layer dependence originates from the layer dependence of both components. Should the layer dependence of the electronic bandgap be found out, we would be able to figure out the

layer dependence of the exciton binding energy from the measured excitonic peak position. It is actually very difficult to experimentally or theoretically evaluate the electronic bandgap of MoS₂ with different layer numbers. However, we find out that the layer dependence of the electronic bandgap may be reasonably correlated to quantum confinement effects. The peak position of the *C* exciton E_C in the films thicker than 7 layers shows a linear dependence on $1/L^2$ (Fig. 3b), and can be fitted by the conventional model of infinite quantum wells as $E_C = E_g + R_y + \pi^2 \hbar^2 / 2m_{\text{eff}} L^2 - R_y$. where E_g is the position (optical bandgap) of the *C* peak in bulk MoS₂ materials ($E_g = 2.695$ eV as measured in Fig.1b), R_y is the exciton binding energy and assumed not changing with the thickness in the model of infinite quantum wells, and m_{eff} is the reduced electron-hole effective mass of the film. The introduction of R_y in the equation is to illustrate that the optical bandgap is equal to the electronic bandgap (the first three terms) minus the exciton binding energy (the last term). The fitting to the experimental results (the red lines in Fig. 3a-b) gives $E_C = 2.695$ eV + $150.9/L^2$, from which we can derive the reduced effective mass $m_{\text{eff}} = 0.250 m_0$ for the *C* extions in bulk MoS₂ and the films thicker than 7 layers. We can also derive the exciton binding energy $R_y = 58.9$ meV and Bohr radius $a_b = 1.61$ nm in bulk MoS₂ and thick films, in which the static dielectric constant is set to be 7.6 as measured for bulk MoS₂ previously²⁵.

The peak position E_C in the films thinner than 5-7 layers shows apparent deviation from the model of infinite quantum wells (Fig. 3b). Instead, we can fit the experimental results with a model of quantum wells in fractional dimensional space as^{26, 27}

$$E_C = E_g + R_y + \frac{\pi^2 \hbar^2}{2m_{\text{eff}} L^2} \left[\frac{(D-1)}{2} \right]^2 - \frac{R_y}{\left[\frac{(D-1)}{2} \right]^2} \quad (4)$$

where D is the effective dimensionality that is defined by the ratio of the exciton binding energy R_y^* in the films and that of bulk MoS₂ R_y as $\left[\frac{(D-1)}{2} \right]^2 = R_y / R_y^*$. Again, the first three terms of eq. (4)

represent the electronic bandgap and the last term indicates the exciton binding energy. The factor of $[(D-1)/2]^2$ in the third term originates from the change in the effective mass associated with the effective dimensionality. For the films thicker than 7 layers, D is 3 and eq. (4) is then reduced to the equation for infinite quantum wells. By fitting the experimental results with eq. (4), we can have the effective dimensionality D as 1.75, 2.07, 2.30, 2.51, 2.65, and 2.83 for the films in layer number of 1, 2, 3, 4, 5, and 6, respectively. We can then derive the corresponding exciton binding energies using $R_y^* = R_y/[(D-1)/2]^2$ as 0.421 eV, 0.206 eV, 0.139 eV, 0.103 eV, 0.0865 eV, and 0.0704 eV; we can also derive the corresponding Bohr radius of excitons from $a_b^* = a_b(D-1)/2^{26,27}$ as 0.602 nm, 0.861 nm, 1.04 nm, 1.22 nm, 1.33 nm, and 1.47 nm, respectively. These results are plotted in Fig. 3c.

The model we used to fit the experimental result is based on an assumption that the layer dependence of the electronic bandgap can be ascribed to the effect of quantum confinement. This is supported by our experimental results, in particular, the consistence between the observed peak position of the films thicker than 7 layers and what predicted from the model of infinite quantum wells. However, more theoretical and experimental studies would be necessary to provide more rigorous support, which is to our best knowledge expected to very difficult. Nevertheless, the result we obtained by fitting the experimental results using this model seems to be reasonable when compared to the limited number of studies on the exciton binding energy and Bohr radius available in the literature. There is not study that would allow us to systematically crosscheck all of our results. For instance, the binding energy $R_y = 58.9$ meV and Bohr radius $a_b = 1.61$ we derived for the C exciton in bulk MoS₂ and thick films is reasonably consistent with the binding energy and Bohr radius reported for the A exciton in bulk MoS₂, which are 87.2 meV and 1.11 nm, respectively²⁸. Additionally, the Bohr radius (0.602 nm) we derived for the C exciton in monolayer MoS₂ nicely matches the theoretical prediction, ~ 0.5 nm¹⁷. The derived binding energy (0.421 eV) is reasonable compared with what reported for the A exciton, which

is believed to be 0.4-0.6 eV in monolayer MoS₂^{18, 29}.

With the information of the exciton binding energy and radius, the observed layer dependence of the dielectric function can be intuitively understood from a perspective of geometric confinement. Fig. 4 shows the comparison between the size of excitons and the thickness of the film. While the film is highly anisotropic, the size of the exciton is schematically illustrated by the diameter of a sphere anyway. This is because eq. (4), which we used to derive the exciton radius, treats the excitons as spheres in an isotropic space by converting the geometrical anisotropy into fractional dimensionality^{26, 27}. The size of the exciton in bulk MoS₂, 3.22 nm, is close to the thickness of the 5L film, 3.10 nm (Fig. 4a). Therefore, the exciton in MoS₂ films is expected to start experiencing substantial geometrical confinement when the layer number of the film is decreased to 5, which may lead to decrease in the exciton size. Intuitively, a smaller exciton radius can better facilitate the spatial overlap of the electron and hole wavefunctions and subsequently cause larger amplitude in $|U(0)|^2$. The layer-dependent decrease of the dielectric function is expected when the layer-dependent decrease of the excitonic effect offsets or even exceeds the layer-dependent increase of the joint density of states.

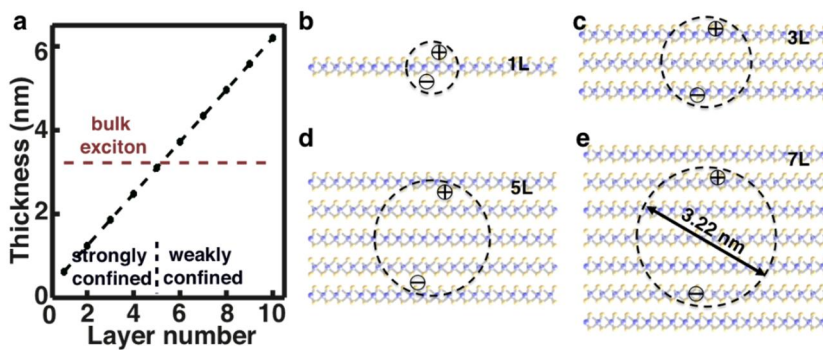


Figure 4. Geometric confinement of excitons in MoS₂ films. (a) Comparison of the size of the exciton in bulk MoS₂ with the thickness of MoS₂ films. The regime where the film is thinner than the exciton size is categorized as strong confinement. (b-e) Schematic illustration of the size of excitons in the films with different layer numbers.

The main conclusion we draw from the analysis of the *C* exciton, i.e. the dominance of excitonic effects in the dielectric function, can be applied to the *A* and *B* excitons as well due to the similar layer dependence in corresponding dielectric functions (Fig.1c-d). However, it is difficult to quantitatively extract the binding energy and Bohr radius for the *A* and *B* excitons as what we did for the *C* exciton. This is because that the positions of the *A* and *B* excitons do not show substantial layer dependence as what observed as the *C* exciton, which makes the fitting by the intuitive model difficult. One reason for the less layer dependence observed at the *A* and *B* excitons could be related with the random variation of the position of the *A* and *B* excitons due to local doping effect from the substrate, which may be as large as ~ 10 meV³⁰. Another reason could be related with the better localization of the *A* and *B* excitons in the plane of the film, which may lead to a less dependence on interlayer interactions³¹.

While our work mainly focuses on MoS₂, we believe that similar dominance of excitonic effects in the dielectric function could generally exist in all the atomically thin semiconducting TMDC materials. Our result bears significant implications for the development of photonics devices with 2D TMDC materials. The obtained dielectric function and refractive index (Table S1) for the MoS₂ with different layer numbers can be immediately useful for the rational design of photonic devices. In particular, as excitons are subject to influence of electric or magnetic fields, the dominance of excitonic effects in the dielectric function makes atomically MoS₂ films an unprecedented platform that may enable the development of field-effect photonics, whose optical functionalities would be tuned by external electric or magnetic fields.

Acknowledgements

This work was supported by a Young Investigator Award from the Army Research Office (W911NF-13-1-0201). Y.C. and Y.Z. gratefully acknowledge the use of computing resources at the A*STAR

Computational Resource Centre, Singapore. H.P. and C.G.V.d.W were supported by the U.S. Department of Energy, Office of Science, Basic Energy Sciences, under Award DE-FG02-07ER46434.

Author contributions

L.Y. conceived the idea. Yiling Yu performed most of the ellipsometry measurements and other characterizations of the films, Yifei Yu synthesized the films. A. G. performed the transfer of the film and some of the AFM measurements. W. L. and N. V. N. helped with part of the ellipsometry measurements. Y. C. and Y. Z. conducted the theoretical calculations. H. P. and C. G. V. d. W also contributed to the theoretical calculations. L. Y., Yiling Yu, and D. E. A. analyzed the results. L. Y. and Yiling Yu wrote the paper. All the people were involved in reviewing the paper.

Competing financial interests

The authors declare no competing financial interests.

References

1. Cao, L.Y. Two-dimensional transition-metal dichalcogenide materials: Toward an age of atomic-scale photonics. *Mrs Bull* **40**, 592-599 (2015).
2. Mak, K.F. et al. Tightly bound trions in monolayer MoS₂. *Nat Mater* **12**, 207-211 (2013).
3. Mak, K.F., Lee, C., Hone, J., Shan, J. & Heinz, T.F. Atomically Thin MoS₂: A New Direct-Gap Semiconductor. *Phys Rev Lett* **105** (2010).
4. Splendiani, A. et al. Emerging Photoluminescence in Monolayer MoS₂. *Nano Lett* **10**, 1271-1275 (2010).
5. Wang, Q.H., Kalantar-Zadeh, K., Kis, A., Coleman, J.N. & Strano, M.S. Electronics and optoelectronics of two-dimensional transition metal dichalcogenides. *Nat. Nanotech.* **7**, 699-712 (2012).
6. Xu, X., Yao, W., Xiao, D. & Heinz, T.F. Spin and Pseudospins in Layered Transition Metal Dichalcogenides. *Nature Physics* **10**, 343–350 (2014).
7. Smith, D.R., Pendry, J.B. & Wiltshire, M.C.K. Metamaterials and negative refractive index. *Science* **305**, 788-792 (2004).
8. Miller, D.A.B. Quantum Mechanics for Scientists and Engineer. (Cambridge University Press, New York, NY; 2008).
9. Palik, E.D. Handbook of Optical Constants of Solids. (Academic Press, London; 1985).
10. Yu, Y.F. et al. Controlled Scalable Synthesis of Uniform, High-Quality Monolayer and Few-layer MoS₂ Films. *Sci Rep-Uk* **3** (2013).

11. Yim, C. et al. Investigation of the optical properties of MoS₂ thin films using spectroscopic ellipsometry. *Appl. Phys. Lett.* **104**, 103114 (2014).
12. Liu, H.-L. et al. Optical properties of monolayer transition metal dichalcogenides probed by spectroscopic ellipsometry. *Appl. Phys. Lett.* **105**, 201905 (2014).
13. Tompkins, H.G. & Irene, E.A. Handbook of Ellipsometry. (William Andrew, Norwich, NY; 2005).
14. Beal, A.R. & Hughes, H.P. Kramers-Kronig Analysis of the Reflectivity Spectra of 2h-MoS₂, 2h-MoSe₂ and 2h-MoTe₂. *J Phys C Solid State* **12**, 881-890 (1979).
15. Komsa, H.-P. & Krasheninnikov, A.V. Effects of confinement and environment on the electronic structure and exciton binding energy of MoS₂ from first principles. *Phys. Rev. B* **86**, 241201 (2012).
16. Kozawa, D. et al. Photocarrier relaxation pathway in two-dimensional semiconducting transition metal dichalcogenides. *Sci. Rep.* **5**, 4543 (2014).
17. Qiu, D.Y., Jornada, F.H.d. & Louie, S.G. Optical Spectrum of MoS₂: Many-Body Effects and Diversity of Exciton States. *Phys. Rev. Lett.* **111**, 216805 (2013).
18. Shi, H.L., Pan, H., Zhang, Y.W. & Yakobson, B.I. Quasiparticle band structures and optical properties of strained monolayer MoS₂ and WS₂. *Physical Review B* **87** (2013).
19. Lee, Y.H. et al. Synthesis of Large-Area MoS₂ Atomic Layers with Chemical Vapor Deposition. *Adv Mater* **24**, 2320-2325 (2012).
20. Li, W. et al. Broad Band Optical Properties of Large Area Monolayer CVD Molybdenum Disulfide. *Phys. Rev. B* **90**, 195434 (2014).
21. Li, Y. et al. Measurement of the optical dielectric function of monolayer transition-metal dichalcogenides: MoS₂, MoSe₂, WS₂, and WSe₂. *Phys. Rev. B* **90**, 205422 (2014).
22. Chuang, S.L. Physics of Photonic Devices. (John Wiley & Sons, New York, NY; 1995).
23. Miller, D.A.B., Weiner, J.S. & Chemla, D.S. Electric-Field Dependence of Linear Optical-Properties in Quantum-Well Structures - Wave-Guide Electroabsorption and Sum-Rules. *Ieee J Quantum Elect* **22**, 1816-1830 (1986).
24. Weisbuch, C. & Vinter, B. Quantum Semiconductor Structures: Fundamentals and Applications (Academic Press, San Diego; 1991).
25. Evans, B.L. & Young, P.A. Optical absorption and dispersion in molybdenum disulphide. *Proc. R. Soc. Lond. A* **284**, 402-422 (1965).
26. He, X.F. Fractional dimensionality and fractional derivative spectra of interband optical transitions. *Phys. Rev. B* **42**, 11751-11756 (1990).
27. He, X.F. Excitons in anisotropic solids: The model of fractional-dimensional space. *Phys. Rev. B* **43**, 2063-2069 (1991).
28. Fortin, E. & Raga, F. Excitons in molybdenum disulphide. *Phys. Rev. B* **11**, 905-912 (1965).
29. Klots, A.R. et al. Probing excitonic states in suspended two-dimensional semiconductors by photocurrent spectroscopy. *Sci. Rep.* **4**, 6608 (2014).
30. Buscema, M., Steele, G.A., Zant, H.S.J.v.d. & Castellanos-Gomez, A. The effect of the substrate on the Raman and photoluminescence emission of single layer MoS₂. *Nano Res.*, DOI: 10.1007/s12274-12014-10424-12270 (2014).
31. Gurarlan, A. et al. Surface Energy-Assisted Transfer of Centimeter-Scale Monolayer and Fewlayer MoS₂ Films onto Arbitrary Substrates. *ACS Nano* **8**, DOI: 10.1021/nn5057673 (2014).

Supplementary Information

Exciton-dominated Dielectric Function of Atomically Thin MoS₂ Films

Yiling Yu², Yifei Yu¹, Yongqing Cai³, Wei Li⁴, Alper Gurarlan^{1,5}, Hartwin Peelaers⁶ David E. Aspnes², Chris G. Van de Walle⁶, Nhan V. Nguyen⁴, Yong-Wei Zhang³, Linyou Cao^{1,2*}

¹Department of Materials Science and Engineering, North Carolina State University, Raleigh, NC 27695, USA; ²Department of Physics, North Carolina State University, Raleigh NC 27695, USA; ³Institute of High Performance Computing, A*STAR, Singapore 138632; ⁴Semiconductor and Dimensional Metrology Division, National Institute of Standards and Technology, Gaithersburg, Maryland 20899, USA; ⁵Department of Fiber and Polymer Science, North Carolina State University, Raleigh, NC 27695, USA; ⁶Materials Department, University of California, Santa Barbara, CA 93106, USA

* To whom correspondence should be addressed.

Email: lcao2@ncsu.edu

This PDF file includes

Methods

Fig. S1-S12

Table. S1 Tabulated refractive index of MoS₂ films References

S1-S4

Methods

Synthesis of centimeter-scale MoS₂ films. The centimeter monolayer and fewlayer MoS₂ films were grown using a chemical vapor deposition (CVD) process that we have previously developed¹. In a typical growth, 4-20 mg molybdenum chloride (MoCl₅) powder (99.99%, Sigma-Aldrich) and 1g sulfur powder (Sigma-Aldrich) was placed at the upstream of a tube furnace. Receiving substrates (typically sapphire) were placed in the downstream of the tube. Other typical experimental conditions for the growth include a temperature of 850 °C, a flow rate of 50 sccm, and a pressure around 2 Torr. The layer number was controlled by controlling the amount of precursors (MoCl₅) used in the synthesis. We also grow centimeter-scale monolayer MoS₂ films using a similar chemical vapor deposition process but with MoO₃ and sulfur being used as precursors

The composition and structure of the synthesized MoS₂ films were extensively characterized by a variety of tools previously. In this work we mainly focused on characterizing the thickness and surface morphology of the synthesized films with optical microscopes and atomic force microscope (AFM, Veeco Dimension-3000).

Ellipsometry measurements of MoS₂ films. The ellipsometry measurement was performed with Woollam VASE (Variable Angle Spectroscopic Ellipsometer, J.A. Woollam Co.) with a Xenon light source in range of 200-1100nm. Typical incident angle was set at 65⁰, but we confirmed that the incident angle does not affect the resulting dielectric constants. The ellipsometry measurement essentially monitors changes in the polarization state of incident light and the light reflected from the films. It yields two spectral parameters (ψ and Δ) related with the amplitude ($\tan \psi$) and phase Δ of a reflectance ratio ρ , which indicates the ratio of the reflection coefficients for p -polarized (parallel to the plane of incidence) and s -polarized (perpendicular to the plane of incidence) light, $\rho = r_p/r_s = (\tan\psi)e^{i\Delta}$. To retrieve the optical constant from the measured results, we perform regression fitting using the Fresnel's equations of a simple two-layer model that consists of a MoS₂ film on top of a semi-infinite substrate. Precise information of the thickness of the film is required for the fitting, which we have obtained by AFM measurements in experiments. We have also confirmed that the surfaces of all the films studied are atomically smooth (roughness < 1 nm) by the AFM measurements (Fig. S1-S3). The typical fitting for experimental results is given in Fig. S4.

First-principles calculations. Our DFT calculations are carried out using the plane wave code Vienna ab initio simulation package (VASP)² with the generalized gradient approximation (GGA). Spin-orbital coupling calculations using the projector augmented wave method with the Perdew–Burke–Ernzerhof functional (PAW-PBE) and a cutoff energy of 400 eV are performed. The multilayer MoS₂ structures are adopted by the experimental lattice of bulk 2H-MoS₂, and the structures are fully relaxed until the Hellmann-Feynman forces become less than 0.01 eV/Å, by using the van der Waals optB88 functional³ to obtain an accurate description of the dispersion force and the interlayer distance. The first Brillouin zone is sampled with a 15×15×1 Monkhorst-Pack grid and a vacuum region with thickness greater than 15 Å is adopted.

The optical properties are calculated based on independent-particle approximation. The involved unoccupied band number is about 10 times of that of valence bands to achieve the converged dielectric function. The accuracy of the k-point sampling is tested for using 15×15 and 18×18 grid for 1L-3L MoS₂, and the calculated dielectric spectra is shown in Fig. S7. While there are

some discrepancies in the low-energy part between these two k-points sets, good convergence is observed for the “C” peak at around 2.75 eV, consistent with previous work⁴. Similarly, for the SOC effect (Fig. S8), the imaginary part of the dielectric constant for MoS₂ layers from 1L to 5L shows little effect from the SOC.

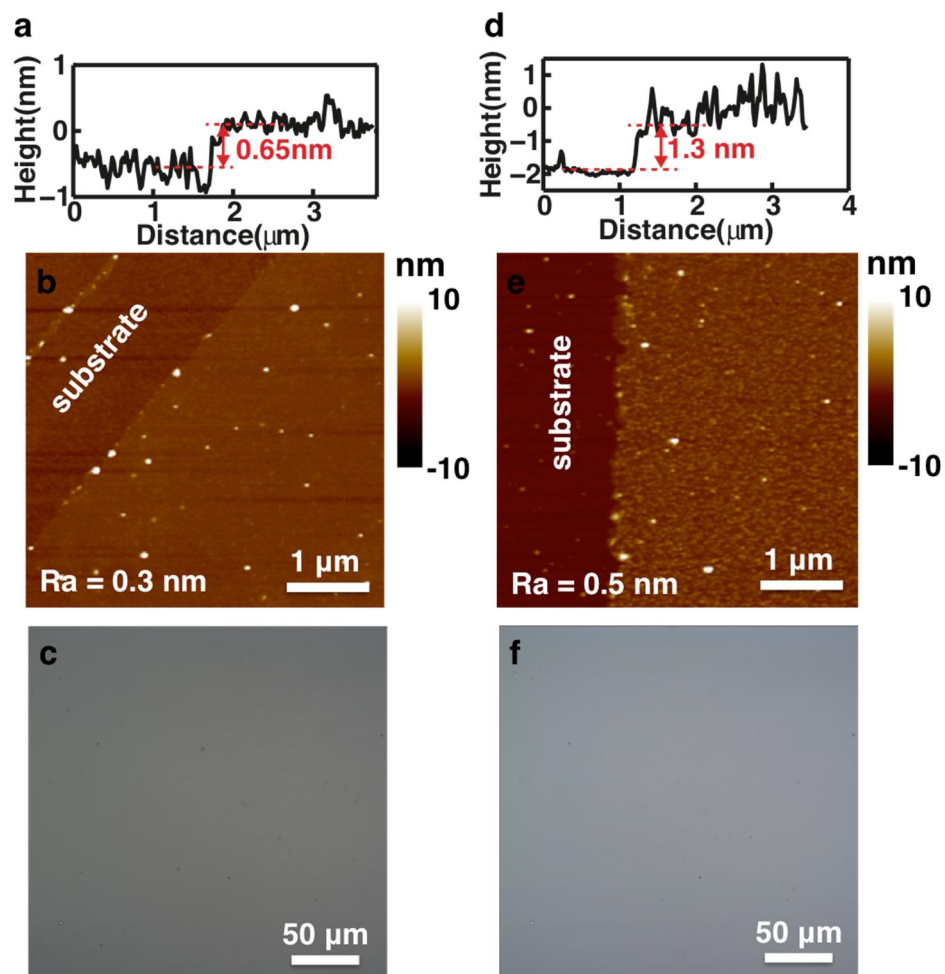


Figure S1. Characterization of monolayer and bilayer MoS₂ films. (a-c) Typical height profile extracted from AFM measurements, AFM image, and optical image of monolayer MoS₂ films. The surface roughness is measured as 0.3 nm as shown in the AFM image. (d-f) Typical height profile extracted from AFM measurements, AFM image, and optical image of bilayer MoS₂ films. The surface roughness is measured as 0.5 nm as shown in the AFM image.

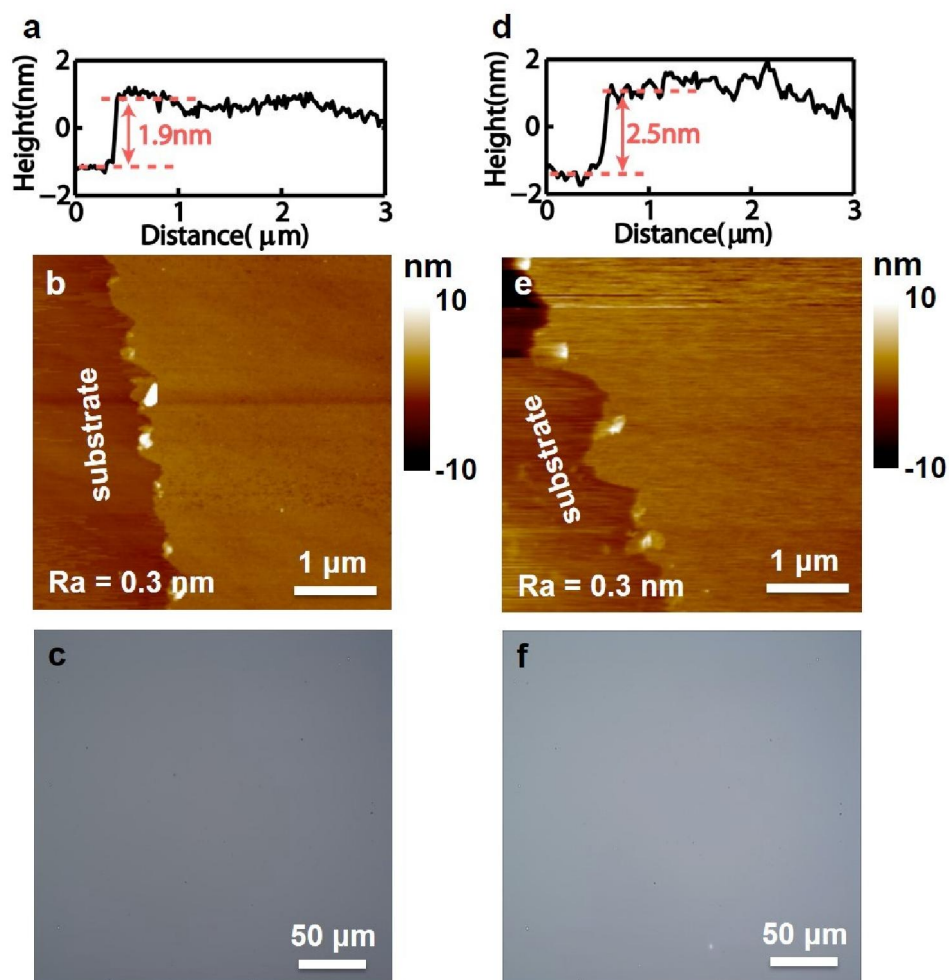


Figure S2. Characterization of three-layer (3L) and four-layer (4L) MoS₂ films. (a-c) Typical height profile extracted from AFM measurements, AFM image, and optical image of 3L MoS₂ films. The surface roughness is measured as 0.3 nm as shown in the AFM image. (d-f) Typical height profile extracted from AFM measurements, AFM image, and optical image of 4L MoS₂ films. The surface roughness is measured as 0.3 nm as shown in the AFM image.

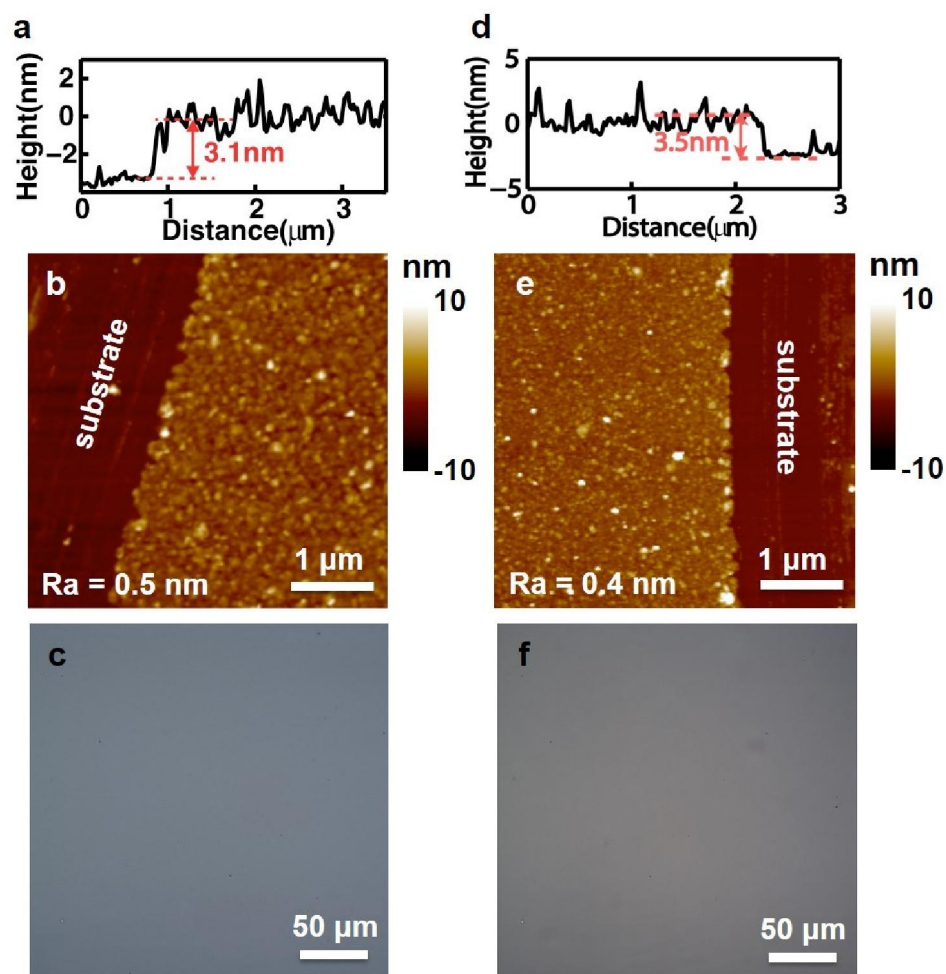


Figure S3. Characterization of five-layer (5L) and six-layer (6L) MoS₂ films. (a-c) Typical height profile extracted from AFM measurements, AFM image, and optical image of 5L MoS₂ films. The surface roughness is measured as 0.5 nm as shown in the AFM image. (d-f) Typical height profile extracted from AFM measurements, AFM image, and optical image of 6L MoS₂ films. The surface roughness is measured as 0.4 nm as shown in the AFM image.

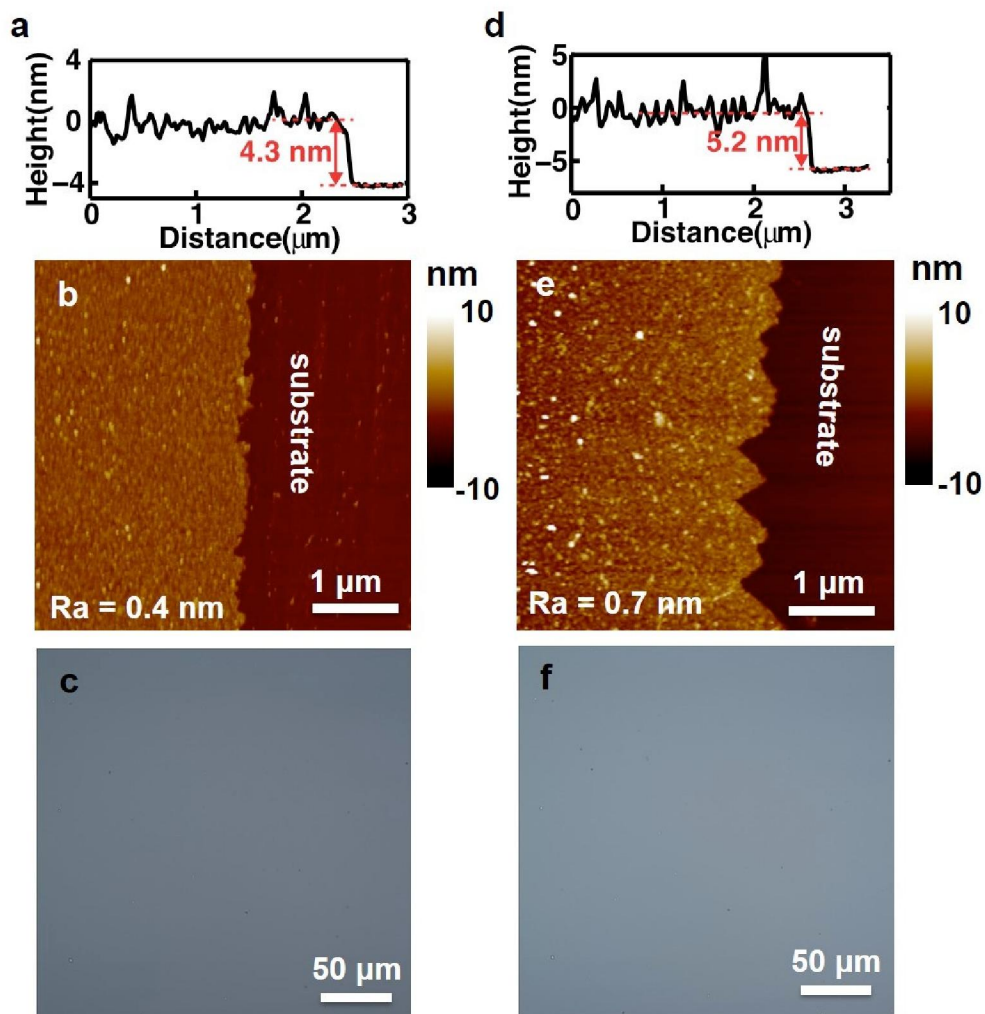


Figure S4. Characterization of seven-layer (7L) and eight-layer (8L) MoS₂ films. (a-c) Typical height profile extracted from AFM measurements, AFM image, and optical image of 7L MoS₂ films. The surface roughness is measured as 0.4 nm as shown in the AFM image. (d-f) Typical height profile extracted from AFM measurements, AFM image, and optical image of 8L MoS₂ films. The surface roughness is measured as 0.9 nm as shown in the AFM image

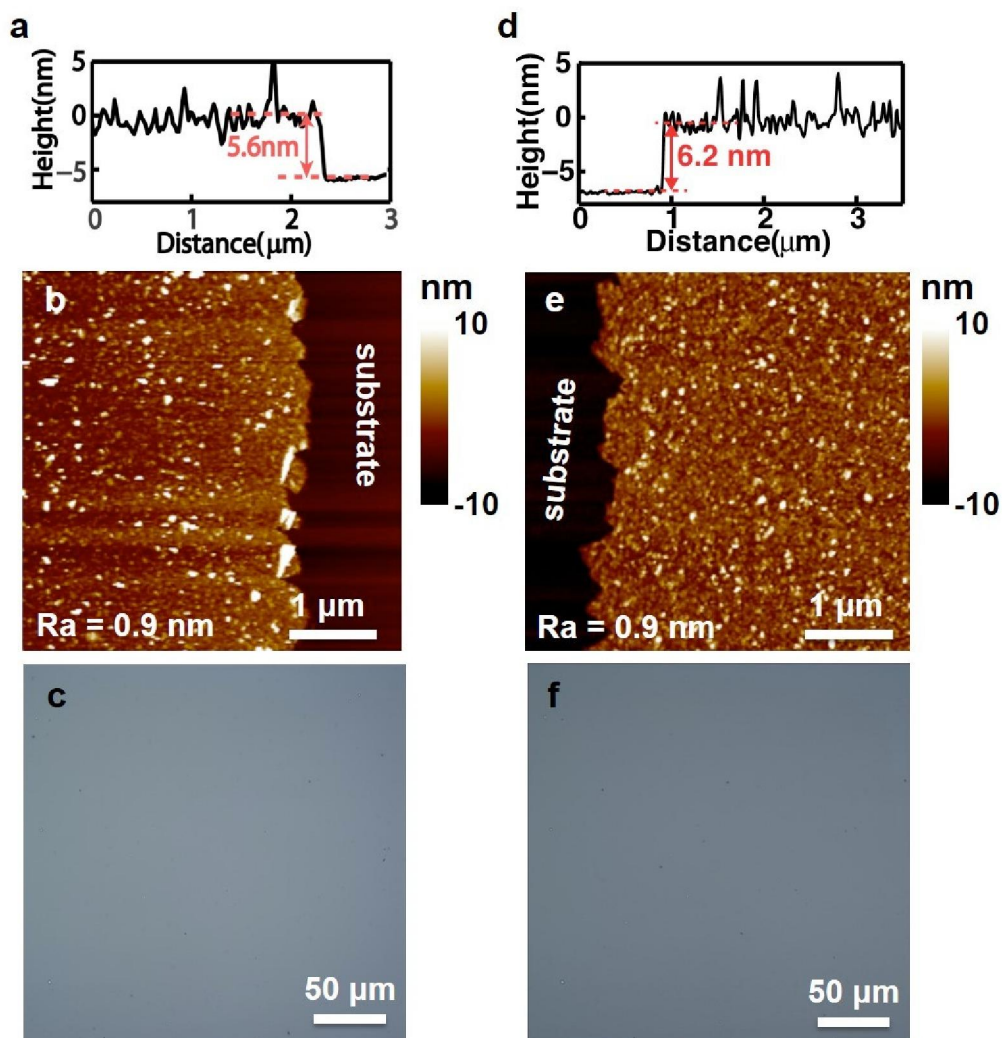


Figure S5. Characterization of nine-layer (9L) and ten-layer (10L) MoS₂ films. (a-c) Typical height profile extracted from AFM measurements, AFM image, and optical image of 9L MoS₂ films. The surface roughness is measured as 0.9 nm as shown in the AFM image. (d-f) Typical height profile extracted from AFM measurements, AFM image, and optical image of 10L MoS₂ films. The surface roughness is measured as 0.9 nm as shown in the AFM image

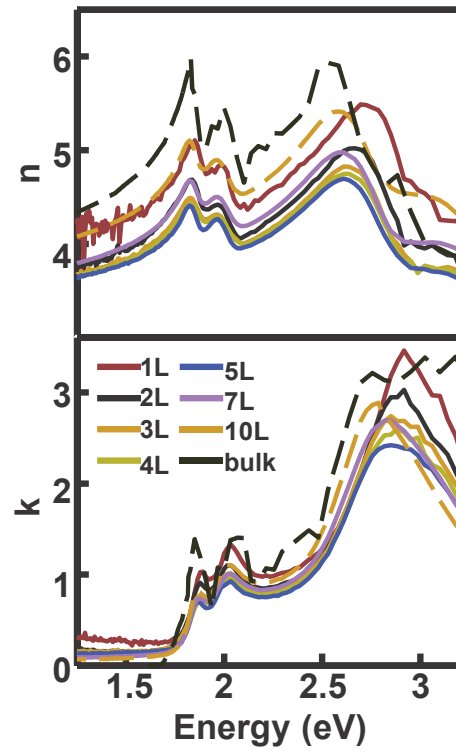


Figure S6. Refractive index of 2D MoS₂. Real (upper panel) and imaginary (lower panel) parts of the dielectric function of 2D MoS₂ vs. layer number. Also given is the refractive index of bulk MoS₂.

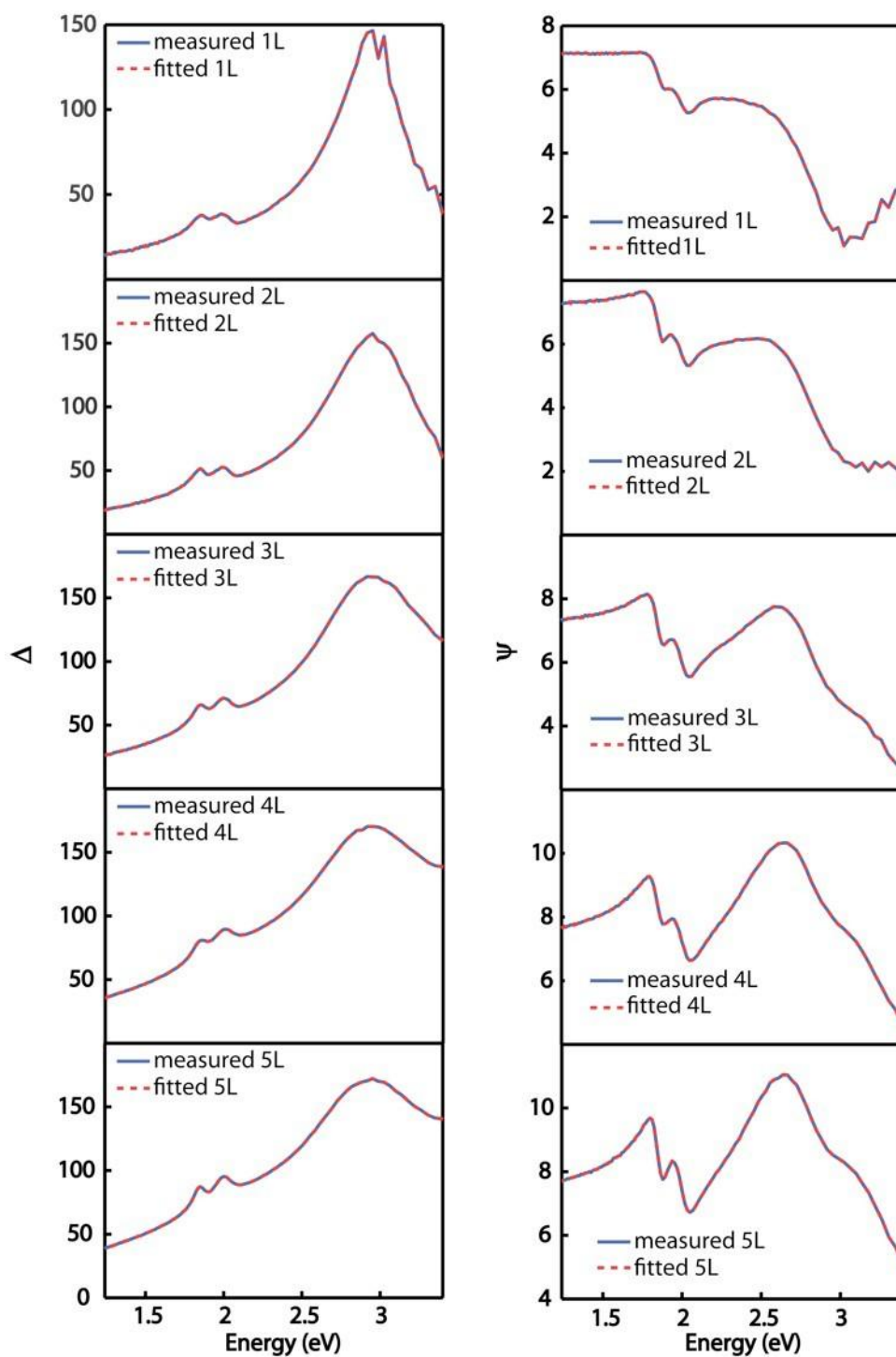


Figure S7. Fitting for the results obtained from ellipsometry measurements. (a) Fitted and measured phase Δ from monolayer to 5-layer MoS2 films. (b) Fitted and measured amplitude ψ for monolayer to 5-layer MoS2 films.

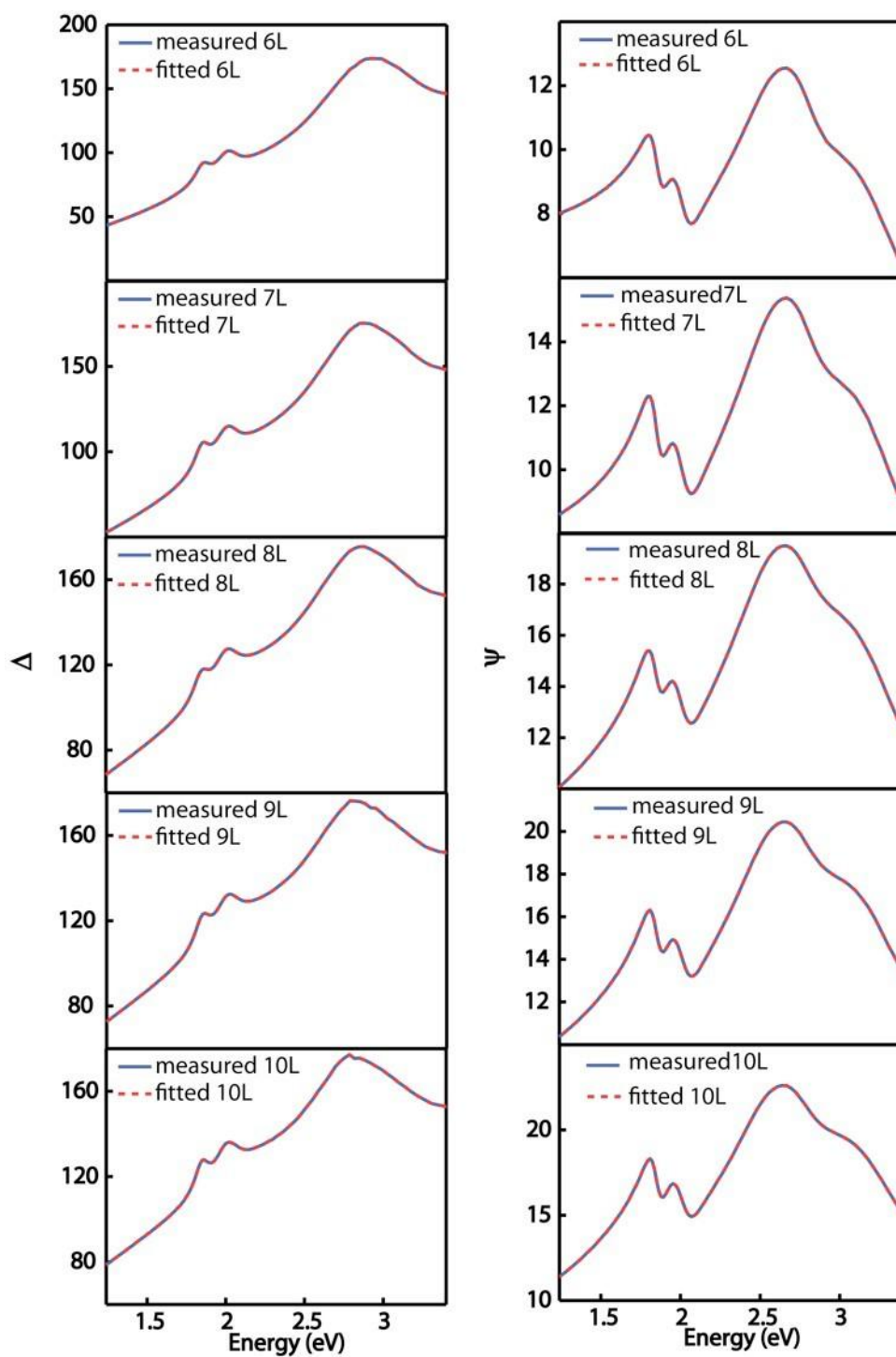


Figure S8. Fitting for the results obtained from ellipsometry measurements. (a) Fitted and measured phase Δ from 6-layer to 10-layer MoS2 films. (b) Fitted and measured amplitude ψ for 6-layer to 10-layer MoS2 films.

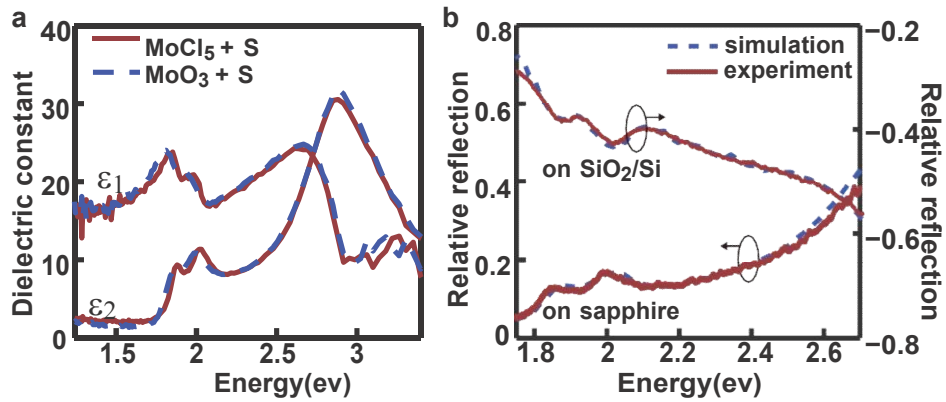


Figure S9. Independence of the measured dielectric function from synthetic processes and substrates. (a) Measured dielectric constants of as-grown monolayer MoS₂ made by two different CVD processes, one using MoCl₅ and S as the precursors and the other using MoO₃ and S as the precursors. The growth substrate in both growths is sapphire. (b) Measured and simulated reflection spectra of monolayer MoS₂ on different substrates, sapphire and silicon with 80 nm thick thermal oxide. The monolayer MoS₂ involved is grown on sapphire substrates and then transferred to SiO₂/Si substrates. The simulation uses the optical constant measured with the as-grown MoS₂ on sapphire substrates.

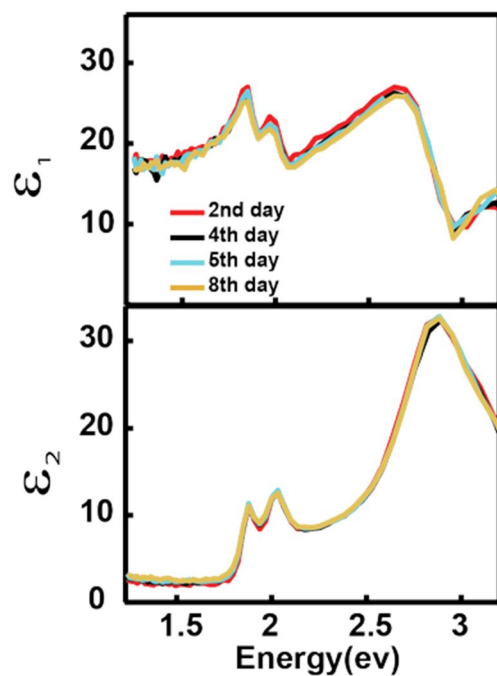


Figure S10. Stability of the dielectric function. Real (upper panel) and imaginary (lower panel) parts of the dielectric function of monolayer MoS₂ measured at different times after synthesis.

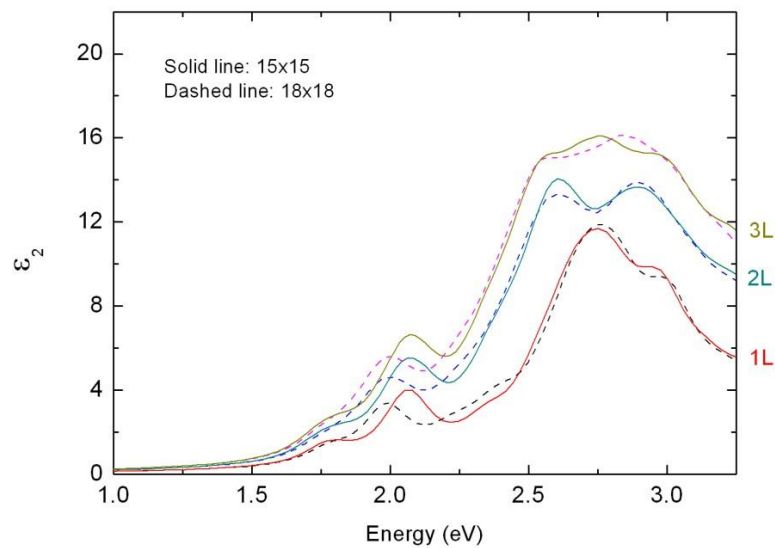


Figure S11. Imaginary part of the dielectric constant for MoS₂ layers from 1L to 3L calculated different k-point sampling.

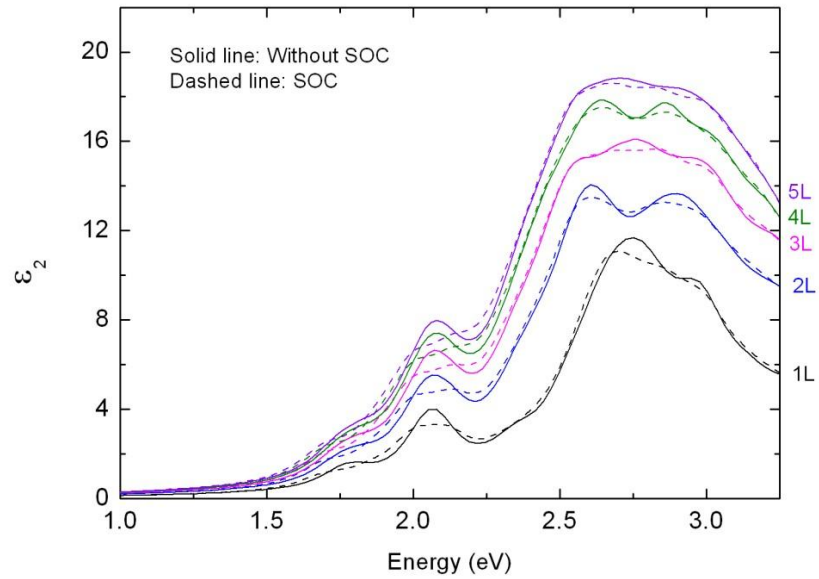


Figure S12. Imaginary part of the dielectric constant for MoS₂ layers from 1L to 5L calculated with spin-orbital coupling (dashed lines) and without spin-orbital coupling (solid lines).

Table S1. Tabulated refractive index of MoS₂ films

wavelength(nm)	1L		2L		3L	
	n	k	n	k	n	k
345	3.035	2.1095	3.1215	1.48	3.1584	1.4242
350	3.3642	1.711	3.1431	1.6304	3.1799	1.3707
355	3.2948	1.7682	3.3188	1.5147	3.1516	1.4211
360	3.0747	2.2111	3.4153	1.4939	3.3381	1.3626
365	3.4136	1.9955	3.482	1.4957	3.3745	1.4535
370	4.0257	1.8186	3.5141	1.636	3.4953	1.5307
375	3.9504	1.964	3.6118	1.6953	3.5514	1.6638
380	4.2656	2.1141	3.7339	1.8568	3.6016	1.8068
385	4.2966	2.2502	3.8891	1.9414	3.6983	1.8775
390	4.241	2.5232	3.8747	2.128	3.7274	1.9909
395	4.2479	2.7103	3.8809	2.3194	3.7528	2.1365
400	4.2558	2.9601	3.9263	2.4171	3.7368	2.2653
405	4.4645	2.9673	3.987	2.4962	3.721	2.4118
410	4.538	3.1094	3.9502	2.6409	3.7648	2.4578
415	4.5785	3.2506	3.9717	2.7826	3.7127	2.6254
420	4.6688	3.3453	4.0257	2.8704	3.816	2.6231
425	4.6942	3.461	3.9825	3.0278	3.889	2.6862
430	4.9523	3.334	4.2523	2.9482	4.0043	2.6842
435	5.1659	3.1845	4.3822	2.9453	4.0705	2.7412
440	5.3321	2.9496	4.5641	2.8467	4.2579	2.6839
445	5.4295	2.7198	4.724	2.6996	4.4327	2.5853
450	5.471	2.5039	4.8808	2.5191	4.5802	2.4602
455	5.4828	2.3085	4.9702	2.3155	4.6858	2.2951
460	5.4897	2.1087	5.0077	2.128	4.7639	2.1338
465	5.4255	1.9334	5.0223	1.9605	4.8122	1.9741
470	5.3851	1.7774	5.0186	1.7949	4.8247	1.802
475	5.3511	1.6549	4.9916	1.648	4.8261	1.6554
480	5.2685	1.5181	4.9396	1.509	4.7934	1.5116
485	5.1999	1.4334	4.9015	1.3921	4.7569	1.3899
490	5.1296	1.3522	4.8236	1.2948	4.7065	1.2803
495	5.0832	1.2878	4.7654	1.2128	4.6505	1.1969
500	5.0093	1.2361	4.7054	1.1513	4.5976	1.1257
505	4.9526	1.1885	4.6687	1.0974	4.5475	1.0737
510	4.918	1.1623	4.6115	1.0532	4.4963	1.0202
515	4.8614	1.1215	4.5572	1.0157	4.4548	0.97899
520	4.8404	1.0768	4.511	0.98054	4.4037	0.93817
525	4.7757	1.0698	4.4642	0.94246	4.354	0.91249
530	4.7458	1.0402	4.4245	0.92324	4.3213	0.89069
535	4.6875	1.0243	4.3847	0.91436	4.2826	0.87048

540	4.6276	1.0169	4.3481	0.8949	4.2396	0.85457
545	4.6184	1.0045	4.3139	0.87514	4.2103	0.84473
550	4.5974	0.98786	4.2807	0.86571	4.1887	0.83567
555	4.5692	0.97655	4.2529	0.8587	4.151	0.82515
560	4.5375	0.98979	4.2331	0.84906	4.1273	0.81697
565	4.4953	0.97569	4.1915	0.84723	4.1036	0.81305
570	4.4593	0.98802	4.1599	0.85819	4.0785	0.8257
575	4.4652	0.99232	4.1311	0.86358	4.0557	0.83162
580	4.4046	1.0283	4.1233	0.86556	4.0351	0.84601
585	4.3665	1.0652	4.0993	0.90042	4.0186	0.85957
590	4.4281	1.1133	4.0773	0.92505	4.0076	0.88298
595	4.3854	1.1736	4.0568	0.98182	4.007	0.91261
600	4.4185	1.2453	4.0802	1.0272	4.0194	0.95695
605	4.4832	1.293	4.1333	1.0777	4.0487	0.98958
610	4.5949	1.3319	4.1995	1.1032	4.1102	1.0138
615	4.7645	1.2887	4.2755	1.1024	4.1728	1.0085
620	4.823	1.2336	4.3632	1.0654	4.238	0.97982
625	4.8473	1.1104	4.405	0.99226	4.2943	0.9388
630	4.8233	1.0397	4.4202	0.93166	4.3156	0.8626
635	4.7608	0.9785	4.4086	0.87284	4.3128	0.80623
640	4.7993	0.9588	4.3911	0.84114	4.295	0.76433
645	4.757	0.94393	4.3689	0.82963	4.2724	0.7384
650	4.7445	0.97564	4.3675	0.84836	4.2619	0.74509
655	4.8177	1.033	4.3777	0.87778	4.2712	0.76408
660	4.9334	1.0246	4.448	0.90742	4.3095	0.77144
665	5.0486	0.94987	4.5632	0.87405	4.373	0.75421
670	5.1062	0.80879	4.6477	0.78976	4.4384	0.70404
675	5.0349	0.67168	4.6851	0.66598	4.4861	0.62352
680	5.0504	0.53835	4.6786	0.54976	4.4922	0.52238
685	4.9719	0.45368	4.6382	0.47019	4.4656	0.42973
690	4.9161	0.39993	4.5794	0.39449	4.4248	0.365
695	4.8819	0.34722	4.5294	0.34297	4.3719	0.31735
700	4.7792	0.31574	4.4932	0.30126	4.3385	0.28054
705	4.7406	0.3121	4.4461	0.27104	4.2891	0.2527
710	4.7011	0.3007	4.4192	0.24924	4.2509	0.23223
715	4.6449	0.28574	4.3796	0.21906	4.2112	0.21784
720	4.6281	0.2684	4.3454	0.20235	4.1777	0.20581
725	4.6008	0.25389	4.3018	0.18963	4.149	0.19284
730	4.5917	0.26534	4.2665	0.18329	4.1269	0.18748
735	4.564	0.25114	4.2493	0.17875	4.1062	0.18071
740	4.4731	0.25553	4.2084	0.17008	4.0695	0.1786
745	4.4781	0.23703	4.1905	0.16271	4.0515	0.17313
750	4.4968	0.26643	4.1663	0.1677	4.0331	0.16169
755	4.4555	0.24217	4.1474	0.16509	4.0284	0.16304

760	4.4546	0.25444	4.1122	0.15967	4.0049	0.1699
765	4.4104	0.25882	4.108	0.15712	3.9894	0.1553
770	4.3872	0.25604	4.0846	0.15634	3.9607	0.1585
775	4.3246	0.2661	4.0686	0.16126	3.9767	0.16305
780	4.3012	0.22656	4.0303	0.15816	3.9409	0.1541
785	4.3975	0.27913	4.0053	0.16128	3.9261	0.15155
790	4.3033	0.23178	4.0308	0.15668	3.8957	0.1591
795	4.3539	0.25401	3.9956	0.15633	3.882	0.16254
800	4.3375	0.2661	3.9946	0.1528	3.8753	0.14879
805	4.2829	0.27118	3.9805	0.15312	3.8912	0.15733
810	4.2618	0.21999	3.963	0.14757	3.871	0.14949
815	4.4143	0.24665	3.9551	0.15666	3.8526	0.15579
820	4.262	0.25912	3.9322	0.16006	3.8459	0.16055
825	4.2599	0.25859	3.9248	0.15353	3.837	0.15222
830	4.2536	0.28422	3.9241	0.14709	3.843	0.15066
835	4.3063	0.27486	3.9432	0.1558	3.8332	0.14969
840	4.2071	0.26591	3.9436	0.15872	3.8175	0.15397
845	4.0152	0.30428	3.9045	0.15062	3.8431	0.14614
850	4.384	0.28634	3.9846	0.16584	3.8452	0.17482
855	4.2731	0.27395	3.9277	0.16079	3.7805	0.1484
860	4.2313	0.29451	3.9019	0.16303	3.8043	0.16181
865	4.0518	0.25802	3.8836	0.16324	3.8042	0.16507
870	4.2107	0.29103	3.8418	0.159	3.7678	0.15209
875	4.1901	0.28231	3.8546	0.15625	3.7828	0.14107
880	4.2146	0.2688	3.8225	0.15519	3.7643	0.16109
885	4.1368	0.26439	3.8191	0.15187	3.7538	0.14589
890	4.2505	0.27241	3.8828	0.15811	3.7618	0.14685
895	4.1246	0.275	3.823	0.15444	3.7427	0.15058
900	4.2324	0.27653	3.8394	0.16086	3.7517	0.15551
905	4.1399	0.29945	3.8437	0.15368	3.7459	0.1452
910	4.0882	0.27867	3.8041	0.14879	3.7418	0.16137
915	4.204	0.27915	3.8372	0.16322	3.7354	0.15593
920	4.2151	0.29217	3.7608	0.1558	3.7179	0.14731
925	4.1818	0.31775	3.8349	0.16625	3.7208	0.15206
930	3.9989	0.27231	3.8169	0.17591	3.727	0.14932
935	4.2799	0.28077	3.8124	0.16884	3.6963	0.15023
940	4.2274	0.30284	3.7828	0.16941	3.6996	0.16622
945	4.3511	0.29421	3.7913	0.16523	3.7445	0.15839
950	4.2508	0.29206	3.7844	0.17303	3.6923	0.15044
955	4.3307	0.29048	3.8152	0.16167	3.7089	0.15293
960	4.1119	0.36195	3.7906	0.17346	3.6594	0.15831
965	3.6847	0.30302	3.7358	0.16777	3.6834	0.16439
970	4.2891	0.30635	3.7615	0.17787	3.6761	0.15848
975	4.2642	0.32016	3.7736	0.18801	3.7132	0.16278

980	4.0643	0.30154	3.7598	0.16946	3.6674	0.15559
985	4.0738	0.30023	3.7561	0.18424	3.6723	0.15389
990	4.26	0.31443	3.8044	0.17347	3.68	0.15773
995	4.1482	0.32433	3.7509	0.18282	3.6638	0.15621
1000	4.1655	0.32855	3.7309	0.1854	3.6428	0.15677

wavelength(nm)	4L		5L		6L	
	n	k	n	k	n	k
345	2.5614	1.8298	3.0358	1.3321	3.0844	1.3501
350	3.194	1.3347	3.0551	1.3281	3.1263	1.3278
355	3.125	1.4035	3.1296	1.3226	3.1888	1.3263
360	3.2429	1.4139	3.2271	1.321	3.2635	1.3337
365	3.2509	1.5094	3.2787	1.3537	3.3504	1.3692
370	3.4527	1.4604	3.3782	1.4042	3.4356	1.4218
375	3.5296	1.5183	3.4467	1.4665	3.5215	1.4918
380	3.5911	1.6489	3.5307	1.572	3.598	1.5798
385	3.6367	1.7441	3.5988	1.6661	3.6692	1.6879
390	3.694	1.8858	3.6456	1.7875	3.7171	1.8181
395	3.7279	2.0512	3.6812	1.9205	3.7502	1.9475
400	3.7228	2.1625	3.7	2.0316	3.7609	2.0817
405	3.7459	2.205	3.7055	2.1543	3.7696	2.1851
410	3.7663	2.3166	3.7282	2.2037	3.7707	2.2849
415	3.689	2.5041	3.716	2.311	3.7685	2.3836
420	3.8204	2.4765	3.7435	2.373	3.8037	2.4242
425	3.825	2.5621	3.8057	2.3871	3.8434	2.4684
430	3.9221	2.6016	3.8774	2.4095	3.9145	2.5102
435	4.0918	2.5361	3.9761	2.4199	4.025	2.5045
440	4.2156	2.5281	4.0915	2.4114	4.1697	2.4642
445	4.3628	2.4465	4.2231	2.3754	4.3019	2.4399
450	4.4941	2.3408	4.363	2.3038	4.4553	2.3357
455	4.6071	2.1983	4.4893	2.1779	4.5806	2.2191
460	4.6802	2.0611	4.584	2.0393	4.678	2.0717
465	4.7282	1.8988	4.6426	1.8974	4.7455	1.9145
470	4.749	1.7469	4.6799	1.7471	4.7787	1.762
475	4.7481	1.6091	4.696	1.5934	4.789	1.619
480	4.7362	1.4717	4.6796	1.4624	4.7778	1.4747
485	4.7031	1.3579	4.6507	1.3532	4.7532	1.3492
490	4.6591	1.2501	4.6138	1.2294	4.7125	1.2375
495	4.6139	1.1679	4.57	1.156	4.6664	1.145
500	4.5608	1.0933	4.5203	1.0741	4.614	1.068
505	4.5105	1.0365	4.4705	1.0094	4.562	1.0016
510	4.4681	0.98793	4.4263	0.95779	4.5105	0.94978
515	4.4167	0.94254	4.3782	0.91445	4.4636	0.90615

520	4.3717	0.91075	4.337	0.87585	4.416	0.86924
525	4.3385	0.87681	4.2945	0.85184	4.3725	0.83965
530	4.2953	0.85398	4.2561	0.82294	4.3307	0.81397
535	4.2566	0.83392	4.2181	0.80078	4.2934	0.79583
540	4.2195	0.82141	4.1836	0.78992	4.2575	0.77728
545	4.196	0.803	4.1526	0.7659	4.2234	0.76694
550	4.1629	0.79384	4.1246	0.76979	4.1946	0.75332
555	4.1337	0.79206	4.0911	0.75762	4.165	0.74949
560	4.1085	0.78915	4.0697	0.75156	4.1388	0.74522
565	4.0855	0.78346	4.0452	0.75376	4.1148	0.74631
570	4.0621	0.78814	4.0281	0.75084	4.0906	0.74932
575	4.0469	0.79079	4.0067	0.76026	4.0728	0.75755
580	4.0238	0.80428	3.9861	0.76684	4.0539	0.7701
585	4.0138	0.81894	3.9703	0.77828	4.0419	0.78739
590	4.0034	0.84196	3.9569	0.79617	4.0334	0.81297
595	4.0026	0.87146	3.9538	0.8258	4.0393	0.8412
600	4.0203	0.91388	3.9554	0.8607	4.0595	0.87293
605	4.0568	0.94228	3.9835	0.90045	4.0972	0.89817
610	4.1131	0.95913	4.0276	0.92813	4.1509	0.9087
615	4.1722	0.94849	4.1008	0.93788	4.2138	0.89697
620	4.2366	0.91014	4.1759	0.91607	4.2678	0.85902
625	4.272	0.85979	4.2334	0.85543	4.3055	0.80191
630	4.287	0.79769	4.2669	0.78154	4.3149	0.74104
635	4.2841	0.74063	4.2544	0.70846	4.3088	0.68818
640	4.2645	0.70184	4.2269	0.65469	4.2849	0.65194
645	4.2443	0.69144	4.1877	0.63311	4.2652	0.638
650	4.2341	0.69161	4.1576	0.6314	4.2554	0.64115
655	4.2472	0.69864	4.1489	0.65775	4.2645	0.65279
660	4.2836	0.70641	4.1709	0.69372	4.3021	0.65914
665	4.3376	0.68971	4.2397	0.70046	4.3599	0.64246
670	4.4007	0.63422	4.3282	0.67378	4.4217	0.58933
675	4.431	0.55125	4.3912	0.58729	4.4573	0.50454
680	4.4362	0.46543	4.4087	0.47751	4.4554	0.41062
685	4.4055	0.37922	4.3839	0.37166	4.4243	0.32837
690	4.3647	0.32056	4.3318	0.30779	4.378	0.26886
695	4.3169	0.27772	4.2695	0.25896	4.3291	0.22579
700	4.2732	0.24239	4.2228	0.22526	4.2818	0.19555
705	4.2329	0.21952	4.1818	0.20342	4.2399	0.17523
710	4.197	0.20274	4.1423	0.19703	4.2011	0.16097
715	4.1634	0.19636	4.1053	0.18286	4.1676	0.15099
720	4.1348	0.18719	4.0859	0.17904	4.1392	0.14232
725	4.1079	0.17553	4.0524	0.17421	4.1128	0.13598
730	4.0839	0.17365	4.0299	0.16416	4.0894	0.13149
735	4.0672	0.16776	4.0156	0.16941	4.067	0.12855

740	4.0394	0.15977	3.9852	0.16233	4.0464	0.1255
745	4.015	0.15476	3.9688	0.16532	4.0261	0.12153
750	4.0067	0.15455	3.9592	0.1583	4.0097	0.11965
755	3.979	0.14984	3.9319	0.15873	3.9921	0.11762
760	3.9687	0.149	3.926	0.15605	3.9749	0.11452
765	3.9546	0.14577	3.9118	0.15454	3.9617	0.11422
770	3.9386	0.14733	3.899	0.14716	3.9498	0.11075
775	3.9217	0.1442	3.8898	0.15178	3.9342	0.10927
780	3.9136	0.13708	3.8721	0.14377	3.9212	0.10985
785	3.9127	0.14229	3.8594	0.14723	3.9133	0.10929
790	3.8948	0.14163	3.8463	0.14252	3.9023	0.10914
795	3.8853	0.14457	3.8369	0.14951	3.8884	0.10814
800	3.8607	0.1339	3.8281	0.14275	3.8839	0.10661
805	3.8493	0.14862	3.8242	0.14704	3.8699	0.10802
810	3.8543	0.13833	3.8152	0.14599	3.8588	0.105
815	3.8419	0.13944	3.8103	0.14411	3.8526	0.10372
820	3.8366	0.1377	3.7904	0.14833	3.8446	0.10301
825	3.8218	0.13384	3.7966	0.13969	3.8375	0.10308
830	3.8188	0.13272	3.7942	0.14769	3.8305	0.10294
835	3.8049	0.1355	3.7772	0.14329	3.8229	0.10139
840	3.7957	0.13606	3.777	0.13432	3.8134	0.10132
845	3.7814	0.14103	3.7651	0.1462	3.8065	0.10206
850	3.7983	0.13817	3.7593	0.14139	3.8024	0.10217
855	3.7873	0.12976	3.7534	0.1437	3.7923	0.097761
860	3.7721	0.12802	3.7489	0.14498	3.7865	0.098688
865	3.7609	0.13967	3.7459	0.13894	3.7829	0.10117
870	3.7525	0.13064	3.7407	0.14129	3.7779	0.10089
875	3.7504	0.13277	3.733	0.13208	3.7697	0.098302
880	3.749	0.13245	3.7339	0.13308	3.7645	0.098093
885	3.7494	0.12771	3.7245	0.13506	3.7597	0.09857
890	3.7507	0.12503	3.7133	0.12863	3.7546	0.098106
895	3.7348	0.12769	3.7121	0.13275	3.7498	0.097763
900	3.7305	0.13342	3.7048	0.13633	3.7443	0.098424
905	3.7231	0.13129	3.7045	0.13451	3.7398	0.097871
910	3.7173	0.13197	3.7065	0.13914	3.7359	0.097249
915	3.7126	0.13251	3.6967	0.13766	3.7313	0.097509
920	3.7056	0.13923	3.6897	0.13257	3.727	0.097305
925	3.7127	0.13301	3.6875	0.13715	3.7229	0.098209
930	3.7068	0.12879	3.6928	0.13281	3.7178	0.097795
935	3.6978	0.12756	3.6761	0.1361	3.7143	0.099327
940	3.6934	0.13052	3.6799	0.12969	3.7109	0.097141
945	3.6914	0.12977	3.6765	0.12749	3.7078	0.09625
950	3.6886	0.13782	3.6737	0.12456	3.7051	0.098084
955	3.6894	0.13452	3.6708	0.13453	3.6999	0.097999

960	3.6857	0.1339	3.66	0.12888	3.6974	0.097411
965	3.6795	0.12964	3.6607	0.13504	3.6908	0.097385
970	3.6736	0.13581	3.6509	0.13255	3.6874	0.096856
975	3.683	0.13931	3.6644	0.13727	3.6842	0.096808
980	3.6674	0.1338	3.6545	0.13241	3.6788	0.097124
985	3.6602	0.13559	3.6325	0.1357	3.6796	0.099659
990	3.6631	0.13305	3.6507	0.13053	3.6755	0.098649
995	3.656	0.13371	3.6474	0.13157	3.6729	0.099293
1000	3.6531	0.13736	3.6341	0.13545	3.6696	0.099894

wavelength(nm)	7L		8L		9L	
	n	k	n	k	n	k
290	3.4972	1.2998	3.6923	1.1447	3.7718	1.0328
295	3.5023	1.367	3.7013	1.178	3.7427	1.1995
300	3.4694	1.394	3.5908	1.3551	3.6599	1.2548
305	3.4036	1.4045	3.551	1.4391	3.6555	1.3201
310	3.336	1.5027	3.5225	1.3941	3.5823	1.3459
315	3.322	1.4274	3.4269	1.4865	3.5416	1.3057
320	3.27	1.479	3.4116	1.5259	3.4668	1.4714
325	3.2837	1.4556	3.4011	1.385	3.4815	1.3729
330	3.2944	1.3648	3.4731	1.3326	3.4809	1.4419
335	3.2633	1.3718	3.3561	1.4464	3.5402	1.3025
340	3.2637	1.3718	3.3961	1.4011	3.494	1.3792
345	3.2641	1.3386	3.4303	1.3006	3.4961	1.2528
350	3.3023	1.3121	3.4685	1.2757	3.5294	1.223
355	3.3719	1.299	3.5294	1.2627	3.5985	1.2029
360	3.4528	1.3035	3.6136	1.2677	3.6826	1.1982
365	3.5462	1.3336	3.709	1.2846	3.7724	1.2182
370	3.6376	1.3899	3.8074	1.3412	3.8714	1.2563
375	3.7289	1.4511	3.9068	1.3996	3.9637	1.3177
380	3.8197	1.5418	4.0057	1.4824	4.0666	1.3915
385	3.8902	1.6507	4.0967	1.5794	4.1601	1.5025
390	3.9566	1.7793	4.1635	1.7226	4.2379	1.6201
395	3.988	1.9267	4.2226	1.8519	4.294	1.7524
400	4.0118	2.062	4.2658	1.989	4.3405	1.8796
405	4.0171	2.1822	4.283	2.1322	4.3609	2.0221
410	4.015	2.2942	4.2965	2.2563	4.3832	2.1277
415	4.0147	2.3961	4.3059	2.3725	4.3728	2.275
420	4.01	2.4927	4.316	2.4728	4.3648	2.4102
425	4.0238	2.5792	4.3299	2.5766	4.4053	2.4629
430	4.0706	2.6375	4.357	2.6694	4.4043	2.5983
435	4.1378	2.6946	4.4244	2.7221	4.444	2.6994
440	4.2652	2.6905	4.5255	2.743	4.5095	2.768

445	4.4052	2.663	4.6486	2.7324	4.5844	2.8411
450	4.5663	2.581	4.7981	2.6589	4.7501	2.7706
455	4.7063	2.4605	4.9346	2.5516	4.8882	2.6874
460	4.8215	2.315	5.0494	2.4198	5.0155	2.563
465	4.9044	2.1545	5.1369	2.2637	5.1158	2.4116
470	4.9532	1.9918	5.1916	2.1083	5.1808	2.2625
475	4.9761	1.8365	5.2233	1.9509	5.2231	2.0897
480	4.9771	1.6824	5.2282	1.7873	5.2387	1.9169
485	4.9572	1.5402	5.2146	1.6371	5.2336	1.7691
490	4.9225	1.4136	5.1826	1.5037	5.206	1.6275
495	4.878	1.3075	5.141	1.3902	5.1648	1.5082
500	4.8251	1.2151	5.0897	1.2925	5.1132	1.3959
505	4.7719	1.1405	5.0342	1.2078	5.0632	1.3087
510	4.7172	1.0777	4.978	1.1377	5.002	1.2349
515	4.6645	1.0258	4.9221	1.0764	4.9488	1.1719
520	4.6139	0.98249	4.8702	1.0307	4.8958	1.1221
525	4.5651	0.94689	4.8203	0.98996	4.8426	1.0836
530	4.522	0.91761	4.771	0.95779	4.7954	1.0463
535	4.4782	0.89218	4.7243	0.93056	4.7499	1.0169
540	4.4403	0.87335	4.6828	0.9099	4.707	0.98963
545	4.4041	0.85673	4.645	0.89235	4.6695	0.9703
550	4.3703	0.84602	4.6095	0.87971	4.6325	0.95709
555	4.3375	0.83775	4.576	0.87198	4.6	0.94654
560	4.3095	0.8319	4.5456	0.8651	4.5676	0.93708
565	4.283	0.83031	4.5171	0.8632	4.541	0.93583
570	4.2577	0.83351	4.4911	0.86544	4.5113	0.93621
575	4.2347	0.84044	4.4695	0.87351	4.4871	0.9397
580	4.2144	0.85344	4.4499	0.88519	4.4684	0.95332
585	4.197	0.87124	4.4335	0.90199	4.4462	0.96934
590	4.1902	0.89627	4.424	0.92556	4.4355	0.99475
595	4.1932	0.92731	4.4263	0.95421	4.4391	1.0275
600	4.2113	0.96158	4.4429	0.98682	4.4556	1.0629
605	4.2497	0.99109	4.4772	1.0156	4.4912	1.0969
610	4.3046	1.0072	4.5292	1.0338	4.5487	1.1162
615	4.3719	0.99878	4.5922	1.0317	4.6197	1.1127
620	4.4325	0.96306	4.6579	1.002	4.688	1.0805
625	4.4818	0.90513	4.7114	0.9479	4.7432	1.0185
630	4.502	0.8389	4.74	0.88053	4.7696	0.9466
635	4.4977	0.77679	4.7446	0.81452	4.7704	0.87832
640	4.4752	0.73226	4.7273	0.76155	4.7502	0.82588
645	4.4491	0.70943	4.7029	0.72954	4.7219	0.79517
650	4.432	0.70719	4.6851	0.7185	4.702	0.79334
655	4.435	0.72109	4.6814	0.72287	4.699	0.80448
660	4.467	0.73742	4.704	0.73177	4.729	0.82186

665	4.5298	0.73315	4.7528	0.72707	4.7919	0.82357
670	4.6078	0.68726	4.8171	0.68928	4.8726	0.78365
675	4.666	0.59454	4.8704	0.61454	4.9433	0.69605
680	4.6761	0.48363	4.8903	0.51437	4.963	0.5781
685	4.647	0.38463	4.8732	0.41919	4.943	0.46674
690	4.598	0.3088	4.8323	0.33856	4.8923	0.38264
695	4.5437	0.25494	4.7814	0.2786	4.8365	0.31781
700	4.4906	0.21878	4.7296	0.23671	4.7787	0.27401
705	4.442	0.19383	4.6795	0.20579	4.7266	0.24176
710	4.3986	0.1754	4.6358	0.18508	4.6804	0.21788
715	4.3601	0.16272	4.5942	0.1686	4.6386	0.20133
720	4.3252	0.15274	4.5574	0.15747	4.5989	0.19057
725	4.2952	0.14619	4.5273	0.14864	4.5628	0.18154
730	4.2678	0.1395	4.4969	0.14141	4.5366	0.1743
735	4.2421	0.13593	4.4708	0.13618	4.5081	0.16678
740	4.217	0.13169	4.4458	0.13096	4.481	0.16298
745	4.1952	0.12704	4.4218	0.12653	4.4563	0.15832
750	4.1743	0.12604	4.4002	0.12364	4.4345	0.15283
755	4.1555	0.12129	4.3803	0.12012	4.4136	0.15051
760	4.1389	0.1201	4.3617	0.1169	4.3922	0.14691
765	4.1227	0.11758	4.3437	0.11588	4.3773	0.14221
770	4.1064	0.11639	4.3282	0.11193	4.3573	0.14208
775	4.0927	0.11393	4.3129	0.11032	4.3438	0.13904
780	4.0796	0.1128	4.2978	0.11047	4.3291	0.1358
785	4.0668	0.11275	4.2846	0.1064	4.3149	0.13477
790	4.0534	0.11062	4.2707	0.10698	4.3012	0.13296
795	4.0397	0.11007	4.2593	0.10523	4.286	0.12998
800	4.0301	0.10719	4.2458	0.10259	4.2751	0.12882
805	4.0179	0.10728	4.2331	0.10131	4.2621	0.12699
810	4.0077	0.10608	4.2227	0.099294	4.2491	0.12501
815	3.9976	0.10568	4.2115	0.097373	4.2399	0.12492
820	3.9891	0.10431	4.2017	0.096565	4.2289	0.12063
825	3.9809	0.10323	4.1931	0.095439	4.22	0.12048
830	3.9721	0.10319	4.1842	0.095125	4.2102	0.11856
835	3.9637	0.10154	4.1749	0.093883	4.1994	0.11879
840	3.955	0.10175	4.1656	0.093628	4.1892	0.11732
845	3.9489	0.10215	4.1581	0.092538	4.1822	0.11646
850	3.9379	0.09965	4.15	0.091605	4.1743	0.11646
855	3.9318	0.10056	4.1397	0.091592	4.164	0.11486
860	3.9243	0.09773	4.1329	0.091321	4.1572	0.1142
865	3.9194	0.097773	4.1253	0.088939	4.1489	0.11333
870	3.9123	0.096894	4.118	0.089321	4.1426	0.11253
875	3.906	0.096658	4.1108	0.086885	4.1345	0.11163
880	3.8986	0.095618	4.1026	0.086427	4.1266	0.10953

885	3.892	0.09492	4.097	0.086398	4.1205	0.10868
890	3.8872	0.095464	4.0899	0.086771	4.1144	0.10922
895	3.8807	0.093879	4.0835	0.08629	4.1077	0.1072
900	3.8756	0.093993	4.0769	0.085472	4.1013	0.10737
905	3.8676	0.092612	4.0717	0.085391	4.0954	0.10671
910	3.8641	0.094722	4.0659	0.085023	4.0873	0.10872
915	3.8589	0.092782	4.0599	0.085014	4.0827	0.10507
920	3.8547	0.093257	4.056	0.084889	4.0774	0.10645
925	3.85	0.09313	4.0507	0.084378	4.0728	0.10621
930	3.8441	0.092887	4.0461	0.085745	4.0668	0.10531
935	3.8401	0.091613	4.0421	0.084569	4.0631	0.10413
940	3.8355	0.092333	4.0365	0.083004	4.0568	0.10517
945	3.8314	0.092179	4.0302	0.084009	4.0512	0.10484
950	3.826	0.090759	4.0249	0.082722	4.0484	0.10433
955	3.8218	0.09071	4.0196	0.082297	4.0429	0.10295
960	3.8184	0.09035	4.0163	0.083586	4.0382	0.10119
965	3.8119	0.090305	4.0132	0.082068	4.034	0.10269
970	3.8114	0.089903	4.0075	0.08227	4.0285	0.10053
975	3.8056	0.091299	4.003	0.082816	4.0233	0.1022
980	3.8006	0.091263	3.9987	0.082014	4.0206	0.10192
985	3.798	0.090927	3.9955	0.083107	4.0154	0.10174
990	3.7938	0.091766	3.9911	0.08252	4.0111	0.10077
995	3.7913	0.091764	3.9878	0.082941	4.0073	0.1008
1000	3.7867	0.093497	3.9844	0.082239	4.0022	0.10074

10L

wavelength(nm)	n	k
275	3.8889	0.46559
280	3.9301	0.83355
285	3.8389	0.86449
290	3.8264	1.0317
295	3.7683	1.0961
300	3.7541	1.2344
305	3.7127	1.2669
310	3.6691	1.252
315	3.6259	1.275
320	3.5782	1.345
325	3.5906	1.2531
330	3.5811	1.2913
335	3.5242	1.3573
340	3.5243	1.3895

345	3.5694	1.2122
350	3.6053	1.1739
355	3.6695	1.1487
360	3.7566	1.148
365	3.8485	1.157
370	3.9498	1.2021
375	4.0538	1.2517
380	4.1583	1.3426
385	4.2525	1.4359
390	4.3427	1.5527
395	4.4126	1.6849
400	4.4668	1.8126
405	4.4984	1.9556
410	4.5164	2.0879
415	4.5229	2.2223
420	4.5349	2.3319
425	4.5421	2.4486
430	4.5628	2.5578
435	4.6021	2.6651
440	4.6889	2.7158
445	4.7219	2.8865
450	4.8609	2.8627
455	5.0147	2.798
460	5.1515	2.6832
465	5.2829	2.4814
470	5.3587	2.2918
475	5.4033	2.1126
480	5.4136	1.9448
485	5.4078	1.7579
490	5.3769	1.6211
495	5.33	1.4952
500	5.2755	1.377
505	5.2115	1.2789
510	5.1501	1.2042
515	5.0907	1.1464
520	5.032	1.0924
525	4.976	1.0438
530	4.9239	1.0179
535	4.8733	0.98939
540	4.8288	0.95548
545	4.7877	0.94788
550	4.7497	0.93046
555	4.7173	0.91882
560	4.6814	0.91307

565	4.6495	0.90966
570	4.6224	0.90747
575	4.593	0.91041
580	4.5699	0.92088
585	4.549	0.94077
590	4.5356	0.97007
595	4.536	1.0036
600	4.5524	1.0479
605	4.59	1.0794
610	4.6502	1.1032
615	4.7286	1.1016
620	4.8042	1.0707
625	4.8661	1.0051
630	4.8941	0.9276
635	4.8926	0.84516
640	4.8683	0.78793
645	4.8297	0.75324
650	4.8004	0.75122
655	4.7931	0.77326
660	4.8199	0.80189
665	4.8913	0.81809
670	4.9919	0.78371
675	5.0777	0.68249
680	5.1046	0.55076
685	5.0776	0.42479
690	5.0175	0.32756
695	4.9536	0.26415
700	4.891	0.21591
705	4.837	0.18612
710	4.7828	0.16645
715	4.7347	0.14724
720	4.6958	0.13861
725	4.6612	0.12378
730	4.6303	0.12181
735	4.5992	0.11637
740	4.5678	0.11279
745	4.5464	0.1092
750	4.5231	0.10622
755	4.4982	0.10033
760	4.4776	0.10159
765	4.46	0.095861
770	4.4429	0.096327
775	4.4271	0.092949
780	4.4096	0.092671

785	4.3944	0.0904
790	4.3814	0.089364
795	4.3657	0.089596
800	4.3543	0.085195
805	4.3403	0.086865
810	4.3274	0.08522
815	4.3174	0.081597
820	4.3074	0.080824
825	4.2978	0.081814
830	4.2874	0.080366
835	4.2757	0.077703
840	4.2655	0.078495
845	4.2572	0.081157
850	4.2466	0.077832
855	4.2395	0.079486
860	4.2321	0.078655
865	4.2248	0.075373
870	4.2151	0.07729
875	4.2097	0.074161
880	4.2004	0.071378
885	4.1926	0.072436
890	4.1867	0.073229
895	4.1784	0.071606
900	4.1725	0.074564
905	4.1657	0.07173
910	4.158	0.070905
915	4.1541	0.07066
920	4.1469	0.071455
925	4.1423	0.070668
930	4.1391	0.070459
935	4.1314	0.071227
940	4.1272	0.070284
945	4.1227	0.070336
950	4.117	0.068629
955	4.1106	0.068798
960	4.1089	0.070415
965	4.1046	0.069971
970	4.0976	0.070051
975	4.0931	0.068335
980	4.0894	0.067586
985	4.0849	0.068757
990	4.0802	0.067641
995	4.0755	0.067518
1000	4.0732	0.068066

References

- S1 Yu, Y. F. *et al.* Controlled Scalable Synthesis of Uniform, High-Quality Monolayer and Few-layer MoS₂ Films. *Sci Rep-Uk* **3**, 1866 (2013).
- S2 Kresse, G. & Furthmuller, J. Efficient iterative schemes for ab initio total-energy calculations using a plane-wave basis set. *Physical Review B* **54**, 11169-11186, (1996).
- S3 Becke, A. D. Density-Functional Exchange-Energy Approximation with Correct Asymptotic-Behavior. *Phys Rev A* **38**, 3098-3100, (1988).
- S4 Shi, H. L., Pan, H., Zhang, Y. W. & Yakobson, B. I. Quasiparticle band structures and optical properties of strained monolayer MoS₂ and WS₂. *Physical Review B* **87**, 155304 (2013).